



Cite this: *J. Mater. Chem. C*, 2018, 6, 11817

Function-driven design of stimuli-responsive polymer composites: recent progress and challenges

Yang Shi ^a and Zheng Chen ^{*ab}

Stimuli-responsive polymer composites have been extensively investigated due to their diverse structures and functional properties in response to various environmental stimuli. The past few years have witnessed a rapid expansion of design and fabrication of such composites at both the material and system levels, which opens tremendous opportunities not only for fundamental understanding of their structure–property relationships but also for exploring their applications in emerging areas such as electronics, biomedical devices, soft robotics and electromechanical engineering. A systematic understanding of the progress in the constituent materials, properties and applications of these composites is needed to guide future development. Here, we review the most recent progress (post the year 2012) in the material and structure designs of stimuli-responsive polymer composites to understand the state-of-the-art development, with a focus on photo-, electrical- and thermo-responsive composites. The advantages and disadvantages (or limitations) of different types of polymer composites are evaluated according to response-related parameters such as response time and sensitivity to stimuli. In the end, this review is concluded with challenges and perspectives for future design of better polymer composites.

Received 17th June 2018,
Accepted 25th July 2018

DOI: 10.1039/c8tc02980f

rsc.li/materials-c

1. Introduction

Stimuli-responsive polymer composites represent a large class of composite materials that can change their structures and properties in response to various physical and/or chemical stimuli. They have been extensively investigated due to their

^a Department of NanoEngineering, University of California San Diego, La Jolla, CA 92093, USA. E-mail: zhengchen@eng.ucsd.edu

^b Program of Materials Science and Engineering, University of California San Diego, La Jolla, CA 92093, USA



Yang Shi

Dr Yang Shi received her BS degree from the School of Materials Science and Engineering at Dalian University of Technology in 2012 and her PhD degree from Program of Materials Science and Engineering at University of California, San Diego in 2016. She is now a postdoctoral scholar at University of California, San Diego. Her research interests include responsive materials, polymer composites, and electrode materials for energy storage devices.



Zheng Chen

Dr Zheng Chen is an assistant professor in the Department of NanoEngineering and Materials Science Program at University of California, San Diego. He received his BS from Tianjin University (2007) and PhD from UCLA (2012, with Prof. Yunfeng Lu), both in Chemical Engineering. Then he served as a postdoctoral researcher with Prof. Zhenan Bao and Prof. Yi Cui at Stanford University. His research interest lies in the design, synthesis and application of novel functional polymers, nanostructured materials, and their hybrid materials for electronics, energy and environmental applications.

tunable structure and functionality. By wisely selecting polymer matrices and functional additives (*e.g.*, nanostructured carbons, metals, ceramics), desirable mechanical, optical, electrical, thermal and magnetic properties may be achieved due to the strong synergism between the two constituents. Stimuli-responsive polymer composites can be generally categorized based on the type of their environmental stimuli, such as photo-, electrical-, thermo-, magnetic-, pH-, pressure-, humidity-responsive polymer composites, *etc.* Most of the polymer composites studied for electronics, soft robotics and electromechanical engineering applications fall into the first four categories, though there have been growing research interests in pH-,^{1–5} pressure-^{6–8} and humidity-responsive^{9–11} composites because of their potential applications in environmental sensing and biomedical devices.

The past few years have witnessed a rapid expansion of the design and fabrication of stimuli-responsive polymer composites, which opens tremendous opportunities not only for fundamental understanding of their structure–property relationships but also for exploring new applications. Specifically, driven by their unique properties, a diverse range of compositions and structures have been designed to tune the synergistic functions of various stimuli-responsive polymer composites with the purpose of improving their sensitivity, response time, mechanical properties and thermo/chemical stability. A systematic understanding of the progress in the constituent materials, properties and applications of these composites is needed to guide future development. There have been several earlier reviews that surveyed the literature on stimuli-responsive polymers, and these reviews focused more on the intrinsic properties and response behaviors of the polymers. However, the synergies between the polymer matrices and the fillers often endow a wider range of structure tunability and more diverse functions compared with pure polymers.^{12–14} There have been also some other earlier reviews focusing on shape memory polymer (SMP) composites,^{15–17} while a comprehensive study of recent advances in other polymer composites is lacking. Two recent articles have reviewed the materials, structure and architecture of the class of magnetic-responsive polymer composites.^{18,19} Therefore, in this review, we aim to investigate the most recent progress (post the year 2012) in the area of material and structure design of stimuli-responsive polymer composites to understand the state-of-the-art development, with an emphasis on photo-, electrical-, and thermo-responsive composites.

An important goal of this paper is to provide a systematic understanding of the structure–property–function relationship of polymer composites in the above three categories by following their design considerations and response mechanisms. In the sections of photo-responsive and electro-responsive composites, they are classified and investigated according to their response mechanisms. In the section of thermo-responsive composites, we focus mainly on positive temperature coefficient (PTC) materials, which are the most representative type of such composites. Their response mechanism, materials, designs and applications are reviewed and discussed. Furthermore, the advantages and disadvantages (or limitations) of different categories of polymer composites are evaluated according to

response-related parameters such as response time and sensitivity to stimuli. Finally, this review is concluded with challenges and perspectives for future design of better polymer composites.

2. Photo-responsive polymer composites

Photo-responsive polymer composites often have advantages such as remote or wireless control, good scalability and adaptability in harsh environments.²⁰ For most photo-responsive polymer composites, their responsiveness is mainly due to the photothermal effect, which is the production of heat in materials upon photo-excitation. In general, the photo-response is composed of two decoupled processes: photo-thermal conversion and thermal-induced mechanical response (*e.g.*, deformation). The photomechanical behavior has been most widely used as an actuation strategy, and therefore is the main focus of this section. Polymer composites with photomechanical actuation can be categorized into four major groups according to their designs and responsive mechanisms: shape memory polymer (SMP) composites, liquid crystalline elastomer (LCE) composites, pre-strain-sensitive polymer composites, and laminated (bilayer or multilayer) polymer composites. Their photomechanical response mechanisms are based on the shape memory effect of polymers, *trans-cis* isomerization or nematic–isotropic phase transition, expansion/contraction with different pre-strains, and mismatch of the coefficient of thermal expansion (CTE) in different layers, respectively. It is noted that this classification is mainly based on their responsive mechanism rather than materials. For example, laminated polymer composites with mismatch in the CTE may be composed of the SMP or LCE matrix; however their responsive mechanisms are not related to the shape memory effect or phase transition. Ideal photomechanical responsive polymer composites should possess fast response and large strain/high-complexity motion, since the increase in response speed and strain/motion complexity greatly enhances their practical applications. Therefore, the four major categories of polymer composites are carefully evaluated based on these property metrics, which are summarized in Table 1. Since light intensity and/or wavelength are crucial in determining the response of these composites, these parameters are also provided for each example. Their respective response mechanism and examples of applications are discussed in detail.

2.1 Shape memory polymer (SMP) composites

Photo-responsive SMPs can be deformed into predefined temporary shapes and recover their permanent shape upon photo-thermal heating by near infrared (NIR) or visible light radiation. Complex shape changes can be realized such as mimicking the heliotropism and blooming of sunflowers, extension of springs and stents, and grabbing motion of grippers.^{23,47} SMPs are generally composed of a hard segment determining the permanent phase and a soft segment fixing the temporary shape below the transition temperature (T_{trans}).⁴⁸ The fillers such as

Table 1 Photomechanical responsive polymer composites

Polymer composites	Response time	Responsive strain/shape change/motion	Light intensity or wavelength
SMP composites			
Poly(butylene succinate)–poly(ϵ -caprolactone)/multi-walled carbon nanotubes (MWCNTs) ²¹	52 s for shape recovery upon NIR	Curved to flat	320 mW mm ⁻²
Polyurethane (PU)/sulfonated reduced graphene oxide/sulfonated CNT ²²	18 s for shape recovery upon NIR	15.7% contraction	30 mW cm ⁻²
PU/carbon black ²³	160 s for shape recovery upon NIR	Bent to flat, distorted cubic to normal cubic	87 mW cm ⁻²
Poly(methyl methacrylate- <i>co</i> -butyl acrylate)/NaYF ₄ ²⁴	100 s for shape recovery upon NIR	Bent to flat	980 nm
Poly(vinylidene fluoride-hexafluoro propylene) (PVDF-HFP)/graphene oxide (GO) ²⁵	5 s upon visible light	Tumbler movement	54 mW cm ⁻² , 450 nm
Liquid crystalline elastomer (LCE) composites			
LCE/single-walled carbon nanotubes (SWCNT)–silicone ²⁶	10 s actuation, 30 s relaxation	Reversible flat to bent	1.1 W cm ⁻²
LCE/SWCNT ²⁷	40 s actuation, 40 s relaxation	Reversible 25% contraction or flat to bent upon asymmetric radiation	250 mW cm ⁻²
LCE/GO ²⁸	7 s actuation	33.1% contraction	3 W cm ⁻²
LCE/GO ²⁹	3 s actuation	Flat to bent	54 mW cm ⁻² , 450 nm
LCE/gold nanoparticles (AuNPs) ³⁰	5 s actuation, 1.5 s relaxation	Reversible 27% contraction	95 W cm ⁻²
LCE/silver nanoparticles ³¹	15 s actuation, 80 s relaxation	Reversible 29.8% contraction	22 mW cm ⁻²
LCE/conjugated polymers ³²	30 s actuation, 30 s relaxation	Reversible 50% contraction	808 nm
LCE/croconaine dye ³³	30 s actuation, 30 s relaxation	Reversible 25% contraction	808 nm
Azobenzene-containing molecules/gold nanoparticles ³⁴	3.5–9.5 min for <i>cis</i> – <i>trans</i> transition	Theoretical study	365 nm
Azobenzene containing crosslinked liquid crystalline polymer/CNTs ³⁵	50 s <i>trans</i> – <i>cis</i> upon UV light, 140 s <i>cis</i> – <i>trans</i> upon visible light	Reversible flat to bent	100 mW cm ⁻² , 365 nm (UV); 35 mW cm ⁻² , 530 nm (visible)
Pre-strained polymer composites			
Polydimethylsiloxane (PDMS)/MWCNTs ³⁶	1.5 s actuation, 1.5 s relaxation	Reversible expansion/contraction	808 nm
PDMS/graphene ³⁷	1.5 s actuation, 1.5 s relaxation	Reversible expansion/contraction	808 nm
PDMS/MoS ₂ ³⁸	4 s actuation, 10 s relaxation	Reversible expansion/contraction	808 nm
PDMS/graphene nanoplatelets (GNP) ³⁹	3 s actuation	Reversible change in the grating period	220 mW cm ⁻²
Reactive ethylene elastomer (RET)/CNT ⁴⁰	12 s relaxation (reversible), 17 s relaxation (irreversible)	Reversible and irreversible stress modulations	97 mW cm ⁻²
Laminated polymer composites			
PC/SWNTs ⁴¹	1 s actuation, 1 s relaxation	Reversible flat to bent	100 mW cm ⁻²
PC/GO ⁴²	3 s actuation, 5 s relaxation	Reversible flat to bent	106 mW cm ⁻²
PDMS/(GNP)–PDMS ⁴³	3.4 s actuation	Reversible flat to bent	2.95 W cm ⁻²
PDMS/GNP–chromium ⁴⁴	1 s actuation, 3 s relaxation	Reversible flat to bent	550 mW cm ⁻²
PDMS/RGO ⁴⁵	0.4 s actuation, 1.2 s relaxation	Reversible flat to bent, oscillatory motion	808 nm
PDMS/RGO–CNT ⁴⁶	3.6 s actuation, 6.8 s relaxation	Reversible curved to flat	250 mW cm ⁻²

different nanocarbons including CNTs, GO and carbon black in the SMP matrix absorb NIR radiation, convert it to local heat and therefore lead to the recovery of the permanent shape (Fig. 1a and b).²³ The majority of photo-responsive SMP composites are NIR-induced due to the strong photothermal effect of NIR radiation since it can penetrate much in most polymeric materials, with generally less damage to the material, compared with visible light and ultraviolet (UV) light.^{49,50} The penetration depth of NIR can reach 1–2 cm while that of UV light can only reach 20–150 μm .^{51,52} However, such NIR-induced photomechanical response is often irreversible: the temporary shape (predefined) can be turned into the permanent shape upon NIR radiation, while by turning off the NIR radiation, the permanent shape cannot be turned back into the temporary shape, which is known as the one-way shape memory effect.⁵³

Therefore, only the response time needed for a change from the temporary to the permanent shape (denoted as shape recovery) is listed in Table 1. Nevertheless, reversible response has also been achieved. For example, the PVDF-HFP/GO composite film shows reversible tumbler movement due to the broken equilibrium by turning the visible light on and off (54 mW cm⁻², 450 nm).²⁵ In the initial state, the film is simultaneously subjected to gravity and bracing force which keep it in an equilibrium state before light irradiation, while during the unfolding process, the equilibrium of the film is inevitably broken, which leads to the tumbler movement like a tilting doll. This is due to the three crystal phases: permanent shape A, temporary shape B and intermediate shape C, among which two are switchable domains and one is physically crosslinked determining the permanent shape (Fig. 1c). Upon irradiation of visible light,

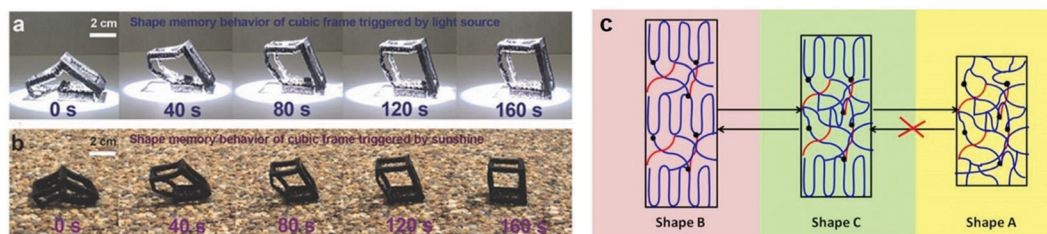


Fig. 1 The shape recovery process of the PU/carbon black cubic frame under (a) 87 mW cm^{-2} of light source (HAL 320, Solar Cell Research solar simulator) and (b) 76 mW cm^{-2} of sunshine. Reprinted with permission from ref. 23. Copyright 2017 John Wiley and Sons. (c) Schematic illustration of the microstructure of the PVDF-HFP/GO nanocomposite film showing the two-way and one-way shape memory effect. Reprinted with permission from ref. 25. Copyright 2015 American Chemical Society.

the temperature rises from $28 \text{ }^{\circ}\text{C}$ to $48 \text{ }^{\circ}\text{C}$, leading to the reversible change from shape B to shape C, while upon NIR irradiation, the temperature rises from $28 \text{ }^{\circ}\text{C}$ to $80 \text{ }^{\circ}\text{C}$, leading to the irreversible change from shape B directly to shape A. Overall, SMP composites show high potential in complex shape change due to the predetermined nature of shapes, especially when 3D printing can be applied in making SMPs.^{23,47,54} However, the one-way shape memory effect limits their applications, since they require a “reset” after the actuation.

2.2 Liquid crystalline elastomer (LCE) composites

LCEs are composed of an elastomeric network with mesogenic moieties attached to the backbones of the polymer network.⁵⁵ The orientation change of the mesogenic units by external stimuli can result in a change of the macroscopic shape.^{56,57} Among different stimuli, the NIR/visible light-induced nematic-to-isotropic phase change (photothermal effect) and the UV light-induced *trans*-to-*cis* isomerization of azobenzene mesogens are two major approaches to trigger the shape changes of LCEs, which will be discussed in detail.

2.2.1 Nematic–isotropic phase transformation. Most of LCE composites are based on nematic–isotropic phase transformation under NIR irradiation. A contraction occurs in these composites during the transformation from the nematic phase with long-range orientational order to the isotropic phase with no long-range orientational order (Fig. 2a).⁵⁸ Different fillers with a photothermal effect have been added to the LCE matrix to trigger this phase transition upon NIR exposure, such as SWNTs.²⁶ A bilayer structure composed of an upper layer of LCE matrix embedded with SWNTs and NIR dyes and a bottom layer of silicone can bend towards the IR radiation direction (Fig. 2b). The embedment of NIR dyes enhances the IR-selectivity, which enables the bending behavior upon 980 nm laser radiation while no response occurs upon 1342 nm laser radiation (Fig. 2c).⁵⁹ Another bilayer structure composed of a polymer-dispersed liquid crystal (PDLC)/GO nanocomposite can bend towards the visible light source (54 mW cm^{-2} , 450 nm) after an exposure of 4 s.²⁹ GO serves as the light absorbent and heat source to thermally induce a phase transition from the LC phase which is rich in the upper layer to an isotropic phase. However, a mechanical stretch must be applied before the exposure to light to induce the mesogenic alignment. Without such a pre-treatment, LC domains will be randomly distributed and therefore no

photomechanical response was observed upon exposure to visible light. This is because there is little shape change during the phase transition from the non-aligned LC to the isotropic phase. It is noted that the bending is not reversible once the light is turned off, and a mechanical stretching step is also needed for returning to the original state. The same group further introduced 4-cyano-4'-pentyloxyazobenzene (5CAZ) into the LC domains, which enabled UV responsiveness due to the nematic–isotropic transformation upon UV light irradiation. This further expanded the responsiveness of PDLC/GO from NIR-responsive to NIR-vis-UV light responsive.⁶⁰

2.2.2 *trans*–*cis* isomerization of azobenzene groups. Azobenzene-containing polymers exhibit contraction under UV irradiation due to the *trans*–*cis* isomerization. It involves a decrease in the distance between the two carbon atoms in position 4 of the aromatic rings from 9.0 \AA (*trans*) to 5.5 \AA (*cis*) (Fig. 2d), which leads to a macroscopic linear contraction of nearly 20%.^{61,62} The isomerization can take place in the pure polymer matrix without adding fillers. Nevertheless, adding certain fillers in azobenzene-containing polymer composites can dramatically accelerate the thermal *cis*-to-*trans* isomerization. Visible light (in particular blue light) and NIR radiation can induce the *cis*-to-*trans* isomerization through thermal relaxation, due to the less stable state and more distorted configuration of the *cis* isomer.⁶³ Therefore, UV radiation and visible light/NIR stimulus are often combined to enable the reversible deformation. Gold nanoparticles (AuNPs) as fillers can effectively decrease the thermal relaxation time of 144–3720 min for the pure azobenzene-containing compound to 3.5–9.4 min for the composite.³⁴ This acceleration comes from the decreased activation barriers of electron attachment and withdrawal with the existence of AuNPs. Since the *trans*–*cis* isomerization occurs in the time scale of less than 1 min,³⁵ the *cis*–*trans* back isomerization becomes the speed limiting step, and therefore its acceleration increases the overall response speed. Another role of the fillers is to achieve a specific bending direction. In an azobenzene-containing crosslinked liquid crystalline polymer (CLCP) with CNT fillers, bending can be realized by the shrinking behavior of the composite surface under UV irradiation (100 mW cm^{-2} , 365 nm).³⁵ The *trans*-to-*cis* isomerization results in a reduction in the orientation of the CLCP mesogens along the CNT-aligned direction, leading to the anisotropic contraction of the surface layer. Upon visible light irradiation

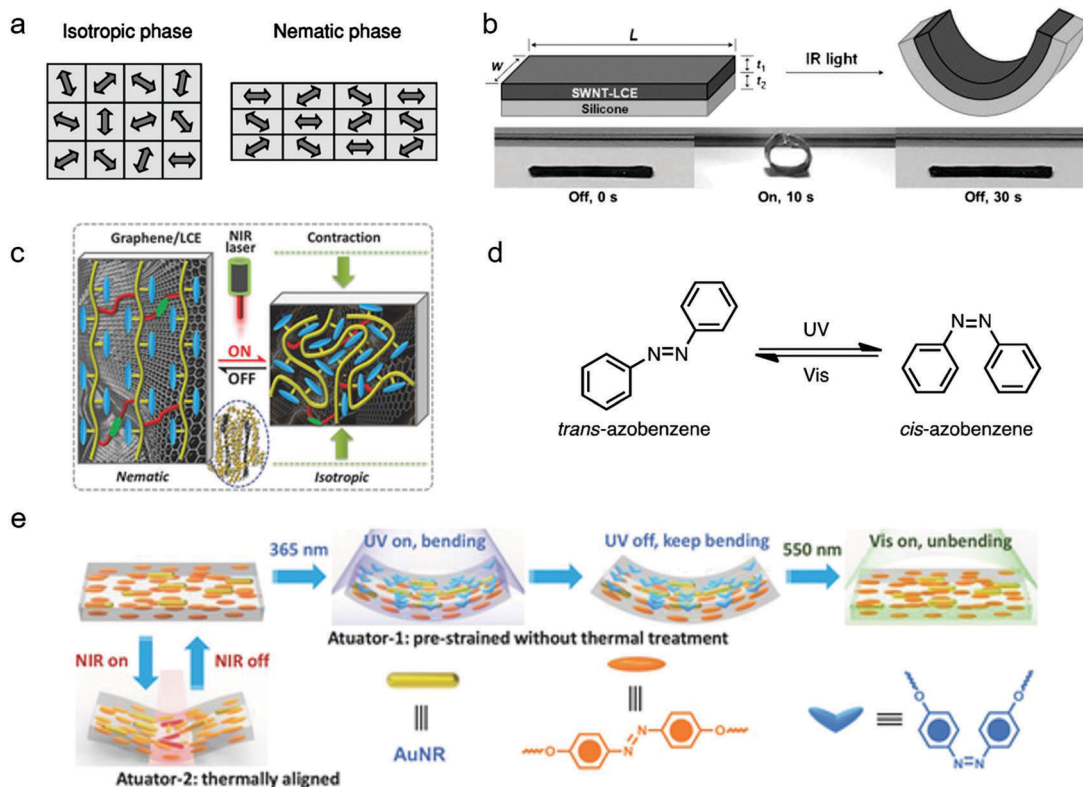


Fig. 2 Examples of photo-responsive LCEs. (a) Schematic illustration of the lattice model for the isotropic–nematic transition in LCEs. In the isotropic phase, the directors are disordered, and there is no strain. In the nematic phase, the directors are ordered along one axis, and the material is extended with strain along that axis. Reprinted with permission from ref. 58. Copyright 2004 American Physical Society. (b) Scheme of a SWNT-LCE composite/silicone bilayer film undergoing bending toward the SWNT-LCE side upon IR irradiation, where L = length and w = width of the bilayer, t_1 = thickness of the SWNT-LCE layer, and t_2 = thickness of the silicone layer. Reprinted with permission from ref. 26. Copyright 2013 John Wiley and Sons. (c) Schematic illustration of reversible photomechanical actuation in graphene/LCE nanocomposites upon on–off switching of NIR light. Reprinted with permission from ref. 59. Copyright 2015 John Wiley and Sons. (d) The *trans*–*cis* isomerization process of azobenzene under UV and visible light. (e) Schematic illustration of the two acting mechanisms for different bending behaviors triggered by UV–vis and NIR light, respectively. Reprinted with permission from ref. 65. Copyright 2015 John Wiley and Sons.

(35 mW cm^{-2} , 530 nm), the *cis*-to-*trans* isomerization enables the bent film to return to the original state. In addition, the CNT fillers increased the tensile strength from 15.7 MPa in the pure film to 31.2 MPa, and also increased the electrical conductivity to 270 S cm^{-1} along the CNT-aligned direction.

By combining the *trans*–*cis* isomerization effect of azobenzene and the photothermal effect of LCE embedded with SWCNT, another azobenzene-containing LCE/CNT composite could realize a bending angle of 60° and a contraction of 25% towards UV and NIR stimulus, respectively.⁶⁴ With a similar concept to combination of azobenzene and the LCE, a liquid crystalline network with AuNR fillers showed both NIR- and UV-light-induced contraction due to the photochemical reaction of azobenzene and the photothermal effect from the surface plasmon resonance of AuNRs (Fig. 2e).⁶⁵ Such bilayer-structured actuators can display photo-controllable bending/unbending (90°) and complex motions as plastic “athletes” that can execute push-ups, sit-ups, as well as crawl forward (13 mm min^{-1}).

2.3 Pre-strained polymer composites

Some polymer composites can expand and contract based on different pre-strains when exposed to IR irradiation. This phenomenon

was first discovered in CNT/polymer composites,⁶⁶ and later found in other carbon or non-carbon/polymer composites, such as PDMS/graphene and PDMS/MoS₂.^{37–39} The mechanism of actuation was proposed to be the ordering of nanotubes induced by the uniaxial extension,⁶⁶ though there remains a need for further justification. The following research was more or less based on such assumption without further investigation of the actuation mechanism, which makes it still an open question. Although pre-strain is not necessary in generating the actuation,⁶⁷ it can determine whether the composites exhibit expansion or contraction. At low pre-strains ($< \sim 10\%$), PDMS/MWCNT composites exhibit expansion upon NIR radiation (808 nm) due to the smaller constant load than the thermoelastic inversion point, while at high pre-strains ($> \sim 15\%$), the composites exhibit contraction upon NIR radiation since the thermoelastic inversion point has been crossed.³⁶ In the study of the dimensional dependence of photomechanical response in PDMS composites, it has been found that as the dimensionality of the nanocarbon additives in the PDMS/carbon polymer decreases, from highly ordered pyrolytic graphite (HOPG, 3D) to graphene nanoplatelets (GNPs, 2D), single-layer graphene (SLG, 2D) and MWCNTs (1D), the NIR-induced photomechanical

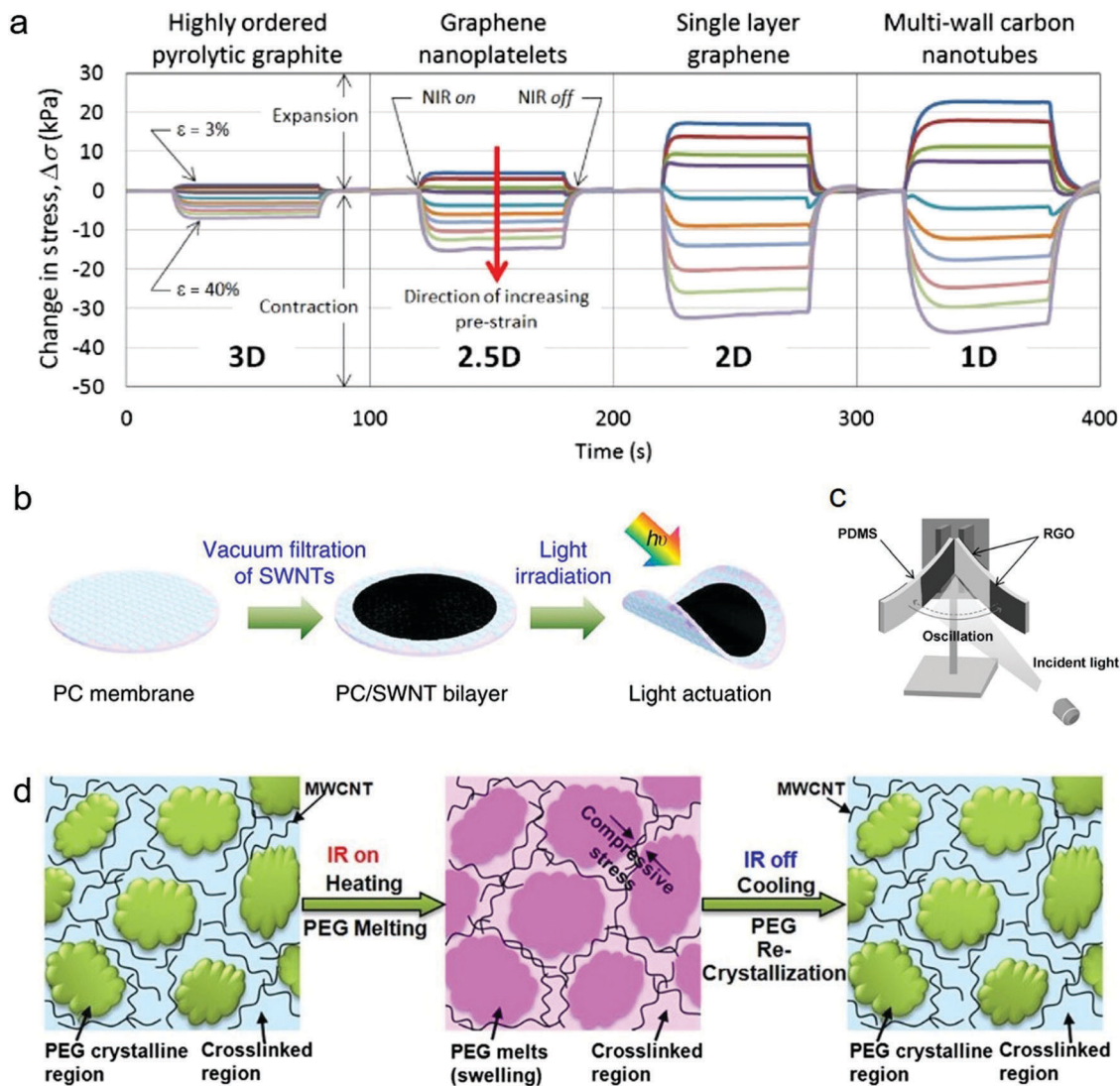


Fig. 3 Examples of pre-strained, laminated and other photo-responsive polymer composites. (a) Photomechanical stress response for 3–40% pre-strains starting with a 3D carbon composite (HOPG/PDMS) and progressing to a 1D composite (MWNT/PDMS) due to NIR illumination. Reprinted with permission from ref. 36. Copyright 2012 IOP Publishing. (b) Schematics illustrating the PC/SWNT bilayer structure in response to photo-stimulation. Reprinted from ref. 41. Copyright 2014 Nature Publishing Group. (c) Schematics illustrating the RGO/PDMS/RGO sandwiched film with oscillation motion due to an incident light. Reprinted with permission from ref. 45. Copyright 2017 John Wiley and Sons. (d) Conceptual illustration of the cyclic, dramatic, and reversible electrical conductivity changes observed in the MWCNT/PCM nanocomposite films regulated by IR. Reprinted with permission from ref. 74. Copyright 2015 American Chemical Society.

stress response increases (Fig. 3a).³⁶ Layer-dependent stress responses to NIR light (808 nm) have been also observed, with a decrease of 20% per additional graphene layer in PDMS/single layer graphene (SLG) composites.³⁷

Particularly, the members of the graphene family, such as graphene, GO and RGO, have also been designed as effective fillers for photo-responsive composites.^{39,67–69} The graphene/poly(styrene-*b*-isoprene-*b*-styrene) composite shows expansion when no pre-strain is applied and contracts under tensile strain conditions on IR radiation.⁶⁷ The loading of graphene in the composite plays a key role in determining the maximal actuating stress (28.34 kPa with 100% pre-strain) upon IR radiation, which is achieved with a graphene loading of 1.5 wt% in this

specific case. This is because the Young's modulus first increases and then decreases with the increased loading of fillers.⁶⁷ The homogeneous distribution of carbon fillers is also important in the photomechanical response. A chemically functionalized graphene (CFG) can be uniformly dispersed in PDMS suspension due to the presence of the long-dodecyl chain.⁷⁰ The composites with 0.05 wt% CFG can exhibit temperature increase due to the photothermal heating effects not only under red light irradiation, but also under short violet light. It has been found that PDMS/thermally reduced graphene oxide (TRGO) composites exhibited higher photomechanical stress than that of the PDMS/CNT composite.⁶⁸ RGO as fillers in chitosan also exhibits contraction when exposed to IR light.⁶⁹ It is not always

the case that the stress response behavior is reversible when different polymer matrices are used. Both the reversible and irreversible stress responses of ethylene terpolymer (RET)/CNT composites were observed, different from the case in PDMS/CNT composites, and the transformation of crystalline domains to amorphous domains in the RET matrix was proposed to explain the irreversible response.⁴⁰ Though such behavior has been mostly observed in polymer composites with carbon fillers, a similar phenomenon was also observed in the MoS₂/PDMS nanocomposite, which shows reversible expansion at lower levels of pre-strains (3–9%) while reversible contraction at high levels of pre-strains (15–50%) upon NIR radiation (808 nm).³⁸

2.4 Laminated polymer composites with mismatch in the CTEs

A bilayer structure has been widely used to achieve photo-responsive bending behaviors due to the mismatch in the CTEs between the two layers. A polycarbonate (PC)/SWNT bilayer film bends towards the CNT side (90°) upon light (white, 100 mW cm⁻²) illumination due to the larger (over 10 times) thermal expansion coefficient of the PC membrane than that of the SWNTs (Fig. 3b).⁴¹ Similarly, a PC/GO bilayer composite bends towards the GO side (a deflection distance of 12 mm for 28 mm-long film) upon NIR radiation (106 mW cm⁻²) due to the larger CTE of PC than that of the GO.⁴² Other than the PC matrix, the composites composed of bilayer PDMS–GNPs/PDMS also showed similar bending behaviors.⁴³ Due to the differences in the CTE and Young's modulus between the two layers, the bilayer platform can be driven to bend towards the PDMS/GNPs side by NIR light irradiation (2.95 W cm⁻²). The same research group also observed two different bending behaviors in this system when the NIR light comes from different sides, *i.e.*, a gradual single-step bending towards the PDMS/GNPs layer upon irradiation from the PDMS side and a dual-step bending (finally bending to the PDMS/GNPs side but with a strong and fast backlash at the time of light on/off) upon irradiation from the PDMS/GNPs side.^{71,72} This is due to the difference in the temperature gradients along the thickness upon irradiation from different sides, caused by the different thermal conductivity (0.45 W m⁻¹ K⁻¹ for PDMS/GNPs *vs.* 0.15 W m⁻¹ K⁻¹ for PDMS) of the two layers.

Similar bilayer structures showed bending towards the materials with lower CTE, such as the composite composed of PDMS/GNP and a chromium layer (lower CTE),⁴⁴ and the composite composed of PDMS and RGO coating (lower CTE).⁴⁵ As another example, a biaxially oriented polypropylene (BOPP) film was attached to a graphite/paper film and the composite bent towards the NIR light due to the much smaller CTE of the paper than the BOPP film.⁷³ Besides the one-directional bending/unbending, an oscillation motion was realized with an RGO/PDMS/RGO sandwiched film: when the RGO side was exposed to NIR light (808 nm), the sandwiched film first bent towards the direction of light; when its back side RGO was exposed to the light, it bent towards the opposite direction (Fig. 3c).⁴⁵ With the same concept, actuation from a closed loop

to flat state or other complex motions can be realized in an RGO–CNT/PDMS composite.⁴⁶

2.5 Other photo-responsive polymer composites

Other photo-responsive polymer composites are more or less related to the photothermal effect. It has been found that the electrical conductivity of CNT/phase change material (PCM) composites showed IR-responsiveness. A CNT/polyethylene glycol (PEG)-triphenylmethanetriisocyanate composite showed IR-regulated electrical conductivity on/off ratios of 11.6 ± 0.6 and 570.0 ± 70.5 at IR powers of 7.3 and 23.6 mW mm⁻², respectively (Fig. 3d).⁷⁴ The change in electrical conductivity is due to the thickness change of the interfacial PCM during the localized PEG melting and recrystallization process between adjacent MWCNTs. In addition, the moisture sensitivity has been combined with the photothermal effect in the design of actuators: a bilayer actuator composed of a polydopamine-modified RGO and a Norland Optical Adhesive (NOA) layer can bend and unbend with periodic NIR radiation.⁷⁵ The polydopamine can absorb water to swell and lose water to shrink due to its hydrophilicity. The RGO sheets convert NIR light into thermal energy, which leads to water loss of the polydopamine. Since the shape of the NOA layer remains unchanged under NIR light, periodic NIR irradiation enables bending/unbending motions of the bilayer actuator. Another photo-responsive nanocomposite based on poly(*N*-isopropylacrylamide) (PNIPAm)/AuNPs hydrogel also demonstrated reversible bending and unbending (~50°) in response to visible light.⁷⁶ This is due to the dramatic reduction in the volume of PNIPAm upon heating, which is also attributed to the photothermal effect of AuNPs.

In summary, the majority of recently developed photo-responsive polymer composites are based on the photomechanical effect and can be classified into four categories according to the response mechanism: SMP composites, LCE composites, pre-strained polymer composites, and laminated (bilayer or multilayer) polymer composites with different CTEs. Even though the light intensity needed to generate the photo-responsiveness may reach as high as 95 W cm⁻², it generally ranges from 20 to 3000 mW cm⁻². Since the response speed and strain/motion complexity are key properties that determine their practical use in photo-responsive devices, the two properties of various composites are compared (Table 1). A figure that generally summarizes these two properties is also shown in Fig. 4. In general, photo-responsive SMP composites can achieve the highest complexity of motion. This is due to the intrinsic properties of SMP since both permanent and temporary shapes are pre-determined, and therefore complicated shape changes and motions can be realized. However, there are two limitations in these SMP composites: slow response and irreversibility. They generally have response time in minutes, though some of them show fast response when the motion is based on a broken equilibrium. The irreversibility of SMP composites has often resulted from the one-way shape-memory effect and a reset is needed after the actuation. LCE composites that are based on nematic–isotropic transformation generally have faster response (mostly 2–40 s) than SMP composites (mostly several minutes),

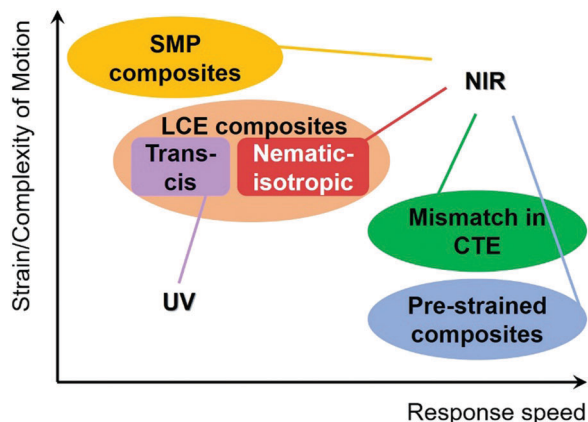


Fig. 4 A general comparison of the response speed and strain/complexity of motion in different categories of photo-responsive polymer composites.

though the majority of them show response time longer than 10 s. However, complicated shape changes and motions can be hardly achieved, and the response generally includes contraction (expansion) and bending (unbending). Even though the response behavior is simple, large strains (25–50%) can be easily generated, with the advantage of reversible response in contrast to SMPs. LCE composites that are based on NIR-responsive nematic–isotropic transformation also show faster response (mostly 2–40 s) than those based on UV-responsive *trans–cis* isomerization (mostly several minutes, with *cis–trans* back isomerization as the speed limiting step). Another limitation of the *trans–cis* isomerization is that the recovery must be induced by direct heat or NIR radiation, which might limit its application when a change of light source is difficult. However, the UV-responsive *trans–cis* isomerization has a unique advantage in applications where high temperature is not allowed and recovery is not required. Pre-strained polymer composites and laminated polymer composites with different CTEs have the shortest response time, and the former type mostly show reversible contraction (expansion) while the latter type mostly show reversible bending (unbending) behaviors. It is tempting to directly compare the strain of LCE composites and pre-strained polymer composites since both of them show reversible contraction and expansion behaviors. However, in the pre-strained polymer composites, researchers often monitored stress change upon light radiation instead of the strain change, because the pre-strain needs to be maintained during the process of light radiation, which makes it difficult to directly compare the contraction (expansion) behavior in such composites with that of the LCE composites.

Based on the above discussion of their photo-responsive properties, it can be recognized that such stimuli-responsive polymer composites can be designed for different applications. SMP composites are suitable in the condition where actuation of complex shape changes or motions is needed while reversibility and fast response are not required. The UV-responsive *trans–cis* composites have unique applications at low temperature when heating of the sample is not desired. Simple and fast motions such as contraction (expansion) or bending (unbending)

can be readily achieved by using pre-strained composites, as well as bilayer (or multilayer) polymers with a mismatch in CTE. More wise design of how the fillers are distributed in the polymer matrix and the combination of different response mechanisms need to be developed for the polymer composites to meet the requirement in various applications.

3. Electro-responsive polymer composites

Electro-responsive polymer composites exhibit shape change, motion or change in mechanical properties in response to electrical stimuli, which can be used in various applications such as actuators, artificial muscles, and control of structural vibrations. Most of the electro-responsive polymer composites can be classified into SMP composites, ionic polymer metal composites (IPMCs), and electrorheological elastomers (EREs). The first two categories of polymer composites transduce electrical energy into mechanical work, and EREs generate a reversible change in modulus under an applied electric field. For both SMP composites and IPMCs, the response time and applied voltage are two key parameters for their practical application. They are summarized in Table 2 followed by the discussion on the response mechanisms and examples of applications of these composites.

3.1 Electro-responsive SMP composites

The mechanism for electro-responsive SMP composites is that the conductive fillers generate heat according to Joule's law, which triggers the shape recovery of SMP matrices.⁷⁷ Generally, when a constant voltage is applied to the composite, a shape change can be induced and monitored. A higher voltage often results in a faster shape recovery.⁸² Similar fillers as those used in photo-responsive SMP composites (Section 2.1) have also been used in these SMP composites to generate Joule heating, such as CNTs.

A higher distribution uniformity and larger volume ratios of CNT fillers in the polymer matrix lead to higher electrical and thermal conductivity, which facilitate faster shape change.⁷⁷ For example, CNTs subjected to ozonolysis followed by UV irradiation show more uniform distribution in a PU/PLA matrix, and the shape of the resultant nanocomposites can be recovered in 15 s after deformation, whereas the pristine composites take 40 s to completely recover their original shape under a voltage of 40 V.⁷⁷ A similar phenomenon has also been observed in PU/PVDF/CNT composites.⁸⁰ The composites filled with ozone-modified CNTs recovered their shape in 15 s, whereas the pristine CNT-filled composites took as long as 30 s. Another benefit is that the modified CNT fillers also increased the tensile strength of polymer composites, from 34.1 MPa of pure PU/PVDF to 90.5 MPa of the composites filled with pristine CNTs, and 108.2 MPa of the composites with ozone-modified CNTs.

Other efforts have been made to modify or decorate the surface of CNTs to achieve faster shape recovery. A SMP composite composed of carbon fibers grafted with carboxylic acid-functionalized

Table 2 Electro-responsive SMP composites and IPMCs

Polymer composites	Response time	Voltage (V)
SMP composites		
Polyurethane (PU)/poly(lactic acid) (PLA)/CNTs ⁷⁷	15 s	40
PU/PLA/MWCNT ⁷⁸	50 s	20
Poly(butylene succinate)-poly(ϵ -caprolactone) (PBSPCL) copolymer/MWCNT ²¹	45 s	75
PU/CNTs ⁷⁹	30 s	40
PU/PVDF/CNTs ⁸⁰	15 s	40
Epoxy-based resin/carboxylic acid-functionalized CNTs grafting onto carbon fiber ⁸¹	40 s	10
Epoxy-based resin/CNTs grafting onto carbon fiber/Nafion-silica nanofiber ⁸²	20 s	5
Epoxy-based resin/carbon nanofiber (CNF)/boron nitride nanopaper ⁸³	74 s	4.8
Epoxy-based resin/Al-grafted carbon fiber ⁸⁴	30 s	6
Epoxy-based resin/Ag nanoparticle-decorated GO ⁸⁵	36 s	8.6
Aerogel/epoxy/CNT/graphene ⁸⁶	120 s	60
Cyanate ester/carbon black/carbon fiber ⁸⁷	143 s	60
Hyperbranched PU/MWCNTs ⁸⁸	9 s	40
Poly(lactic acid) (PLA) plasticized by epoxidized linseed oil (ELO)/MWCNTs ⁸⁹	45 s	40
Poly(L-lactide)-PU/CNT ⁹⁰	180 s at 75 °C	50
Epoxy-based resin/CNT ⁹¹	8 s	17
Poly(ethylene vinyl acetate) (EVA)/poly(ϵ -caprolactone) (PCL)/CNT ⁹²	24 s	20
PLA-ELO/NH ₂ -CNT ⁹³	25 s for 80% shape recovery	40
PLA-ELO/Cu-CNT ⁹⁴	63 s	40
PU/(CNF) ⁹⁵	80 s	30
Epoxy-based resin/carbon felt fiber ⁹⁶	52 s	10
PU/graphene ⁹⁷	10 s	50
Poly(vinyl acetate) (PVAc)/graphene ⁹⁸	30 s	70
Epoxy-based resin/Au ⁹⁹	130 s	14.9
Epoxy-based resin/Au ¹⁰⁰	80 s	13.4
PU/Ag nanowires ¹⁰¹	5 s for more than 80% shape recovery	5
PU/antimony-doped tin oxide/TiO ₂ ¹⁰²	60 s	70
IPMCs		
Sulfonated polyimide/silver ¹⁰³	30 s for 45° bending	0.5
Sulfonated polyphenylsulfone (SPPSU)/Pt ¹⁰⁴	35 s for 90° bending	3
Poly(ether ether ketone) (PEEK)/Pt ¹⁰⁵	35 s for 90° bending	3
Nafion/RGO ¹⁰⁶	40 s for 45° bending	6
Nafion-10-camphorsulfonic acid (CSA)/Nafion-sulfonated montmorillonite (MMT) or polypyrrole (PPy)-coated alumina/Pt ¹⁰⁷	5 s for 45° bending	3
Nafion-carboxylated CNT/palladium ¹⁰⁸	50 s for 35° bending	2
Kraton/GO/Ag/polyaniline (PANI) ¹⁰⁹	40 s for 35° bending	4
RGO/poly(2-acrylamido-2-methylpropanesulfonic acid-co-acrylamide) (poly-(AMPS-co-AAm))/carbon ¹¹⁰	60 s for 30° bending	10

CNTs as fillers shows shape recovery from a “U” shape to a flat shape in 40 s when subjected to a voltage of 10 V, faster than that with the bare carbon fiber fillers (49 s) due to the higher electrical conductivity of the CNT-grafted composite.⁸¹ Nafion/silica nanofibers have been electrospun onto the surfaces of this CNT-grafted carbon fiber to prevent heat dissipation, and therefore have further improved the actuation efficiency (a measure of the conversion rate from electrical energy into electrically resistive heat energy).⁸² In a composite with aluminum (Al) nanopowder-grafted carbon fiber fillers, the siloxane groups were grafted onto the surface of the Al nanopowders to enhance the interfacial bonding between the carbon fiber and the SMP matrix. The Al nanopowders facilitate the transfer of the Joule heating between the carbon fiber and the matrix, which significantly enhanced electrothermal efficiency and shape recovery efficiency, with a large electrical actuation at a voltage as low as 4.0 V (Fig. 5).⁸⁴ Similarly, NH₂-functionalized CNTs also showed enhanced dispersion and surface interaction with the polymer matrix due to the crosslinking between the NH₂-functionalized CNTs and the epoxidized soya oil plasticized-PLA matrix. The results show that the shape memory behavior was

strongly influenced by the weight percent of NH₂-CNT: the recovery time and recovery ratio (%) of the PLA nanocomposite with 3.0 wt% NH₂-CNT were 40 s and 40% under 70 V, respectively, while 5.0 wt% loading of NH₂-CNT helped to reduce the recovery time to 25 s and increased the recovery ratio to 80% under 40 V.⁹³

Besides CNTs^{21,78,79,88–92} and decorated/modified CNTs,^{93,94} other carbon nanostructures such as carbon nanofibers,⁹⁵ carbon fiber felt,⁹⁶ GNP,^{111,112} CNT-graphene,⁸⁶ Ag nanoparticle-decorated GO⁸⁵ and graphene,^{97,98} and non-carbon fillers such as patterned Au electrodes,^{99,100} Ag nanowires,¹⁰¹ TiO₂,¹¹³ and antimony-doped tin oxide/TiO₂¹⁰² have been used as effective fillers in SMPs. The morphology and structure of these filler particles can strongly affect the responsive properties. It has been found that PU with graphene fillers showed higher thermal and electrical conductivity ($1.67 \times 10^{-3} \text{ S cm}^{-1}$, $0.36 \text{ W m}^{-1} \text{ K}^{-1}$) than that with CNT fillers ($2.30 \times 10^{-4} \text{ S cm}^{-1}$, $0.23 \text{ W m}^{-1} \text{ K}^{-1}$),⁹⁷ which could be due to molecular level interactions between PU chains and graphene sheets, leading to a more homogeneous dispersion of nanofillers in the polymer matrix.¹¹⁴ Hexagonal boron nitride (BN) was assembled with CNF and introduced to

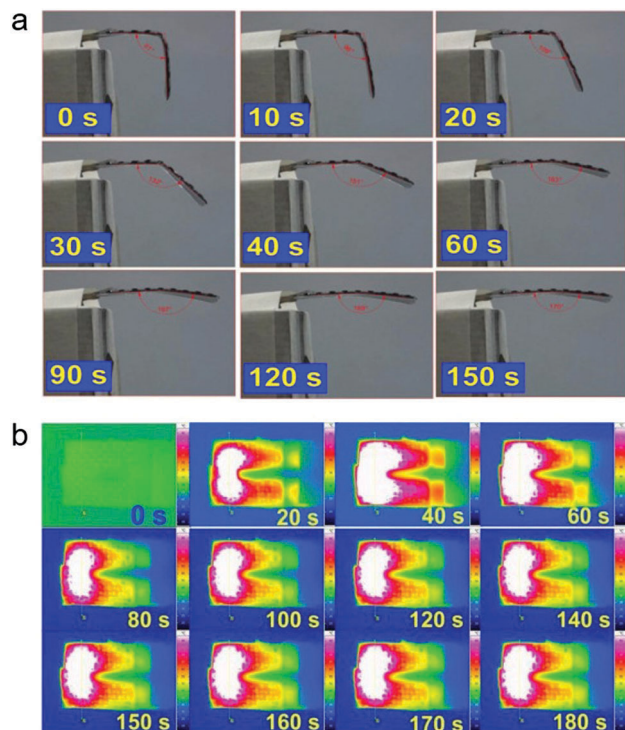


Fig. 5 (a) Snapshot of Joule heating-induced shape recovery of the SMP nanocomposite with aluminum (Al) nanopowder-grafted carbon fiber fillers under an electric voltage of 4.0 V. (b) Snapshot of Joule power heating the SMP nanocomposite monitored using an infrared video camera. Reprinted with permission from ref. 84. Copyright 2015 Elsevier.

improve the thermal conductivity of an epoxy-based fully formable thermoset SMP nanocomposite for enhanced heat transfer and shape recovery.^{83,115,116} A synergistic effect between CNF and BN nanopaper on the shape recovery performance of nanopaper-SMP nanocomposites has been observed for electro-activated shape recovery. A similar effect was also shown in the composite with both carbon black and carbon fiber as fillers, with the former acting as a short-range charge transporter and the latter as a remote charge transporter.⁸⁷

3.2 IPMCs

A typical IPMC has a sandwich structure composed of an ionic exchangeable membrane and two conductive electrodes coated by noble metals, such as Pt, Au, and Ag,¹⁰³ or by nonmetallic nanomaterials such as CNTs,^{117–119} graphene,¹²⁰ RGO,¹⁰⁶ nanoporous carbon,¹²¹ carbon aerogel,¹²² graphene-CNT-Ni,¹²³ and Ag-PANI.¹⁰⁹ The actuation mechanism is mainly based on expansion of the cathode and contraction of the anode, resulting from the migration of cations and water molecules toward the cathode under an electric field (Fig. 6a).^{124,125} When a hydrated strip of IPMC is subjected to a voltage, it undergoes a fast bending deformation towards the anode (positive). Higher voltage leads to larger strain and larger bending angles.^{126–129} Conversely, a voltage can be generated between the two conductive electrodes of IPMC upon mechanical bending due to charge accumulation. These two functions of IPMC can be utilized to develop actuation and sensing capability, respectively.¹⁰⁴

The ionic exchangeable membrane is the most critical component in IPMCs. Among various ionic polymers, Nafion has been the most widely used membrane material in IPMC actuators due to its commercial availability, mechanical robustness, high chemical stability and high proton conductivity.¹⁰⁴ However, some inherent drawbacks still limit its practical applications, such as high cost, environment-unfriendliness, low water-retention capability, and back-relaxation.¹⁰⁴ Back-relaxation is a phenomenon in that the actuation towards the anode is followed by a slow relaxation back to the cathode when subjected to a step input voltage.¹³⁰ This is believed to result from the diffusion of water back to the anode side due to the pressure in the strained regions of the polymer matrix, which pushes water molecules out of the cation-rich clusters.^{131–133} Low-cost sulfonated polyphenyl-sulfone (SPPSU) has been used as an alternative to Nafion, which shows doubled ion exchange capacity (2.23 meq g^{-1}) and 2.5 times higher water uptake (67.2 wt%) compared with Nafion (1.02 meq g^{-1} and 18.7 wt%), respectively.¹⁰⁴ The SPPSU-based actuator offers more rapid bending response (486 ms) than the Nafion-based actuator (3250 ms) while maintaining a comparable maximum strain at 3 V (direct current, DC) (Fig. 6b). Under 3 V sinusoidal voltage at 1 Hz, its maximum strain is approximately twice as that of the Nafion counterpart. However, it shows more serious back-relaxation issue (Fig. 6b). A perfluorinated carboxylic acid membrane, Flemion[®], with higher (40%) ion-exchange capacity (1.44 meq g^{-1}) than Nafion, shows relaxation in the direction of actuation.¹³⁴ This is possibly caused by the migration of the dissociated H^+ with bonded water molecules to the cathode side.¹³⁵ A non-relaxation IPMC has been designed by doping the Nafion matrix with $-\text{COOH}$ groups (attached onto carboxylated CNT), which can generate dissociated H^+ (Fig. 6c).¹⁰⁸ By tuning the CNT content to 2 wt%, a non-relaxation composite can be achieved, though it shows much smaller displacement ($\sim 4 \text{ mm}$) than that with 10 wt% CNT ($\sim 17 \text{ mm}$) (Fig. 6d). Nevertheless, this work provides some insight to further mitigate the relaxation issues by incorporating ion-buffering materials.

Modifications have been also made on the Nafion membrane to increase the displacement and response speed, and to reduce the back-relaxation. A triple-layered IPMC is composed of a Nafion layer containing an amphiphilic organic molecule (10-camphorsulfonic acid; CSA) in the middle section, and two Nafion composite layers containing sulfonated MMT or PPy-coated alumina particles as fillers in the outer sections.¹⁰⁷ The triple-layered IPMCs exhibited 42% higher tip maximum displacements and more rapid response than conventional single-layered Nafion-IPMCs under 3 V voltage, with negligible back-relaxation. The improvement is attributed to higher capacitances, more efficient transport of mobile ions and water, and larger retention of the mobile species in the outer layer composites. It is expected that with further optimization of the membrane structure and composition, larger displacement, faster response and smaller relaxation may be achieved.

3.3 EREs

ERE is the solid counterpart of the electrorheological fluid (ERF). ERF is comprised of polarizable particles dispersed in

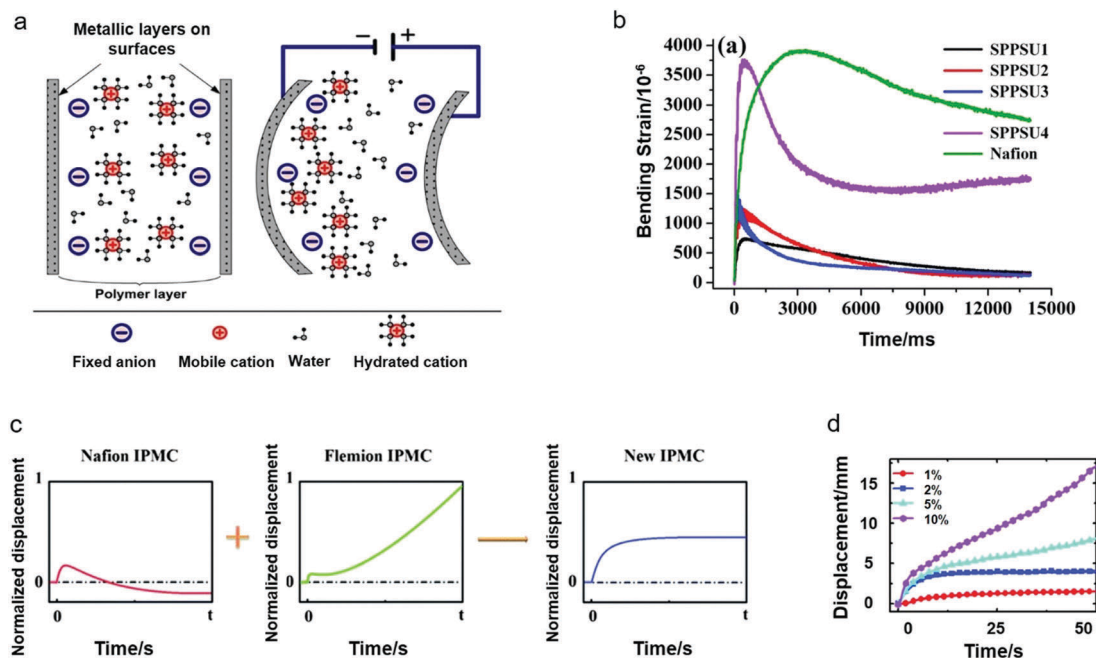


Fig. 6 (a) Working principle of an IPMC actuator. (b) Bending strain as a function of time for various SPSSU-based IPMC actuators in air under a DC voltage of 3 V. Reprinted with permission from ref. 104. Copyright 2014 Royal Society of Chemistry. (c) Illustration of the hypothesis of neutralizing the relaxation deformation of Nafion-IPMC by the slow anode deformation of Flemion-IPMC. (d) The deformations caused by CCNT (obtained by subtracting the deformation of IPMC without CCNT doping from the deformation of IPMC with various CCNT contents). Reprinted with permission from ref. 108. Copyright 2018 Royal Society of Chemistry.

an insulating fluid such as silicone oil or mineral oil. Such fluids can be converted reversibly from a liquid-like to solid-like state by an applied external electric field, because the dipole-dipole interaction between the particles makes them tend to aggregate and form chains/columns along the applied field direction.^{136–140} ERE consists of suspended semiconducting particles in a cross-linkable polymer matrix.¹⁴¹ In response to an applied electric field, the particles aggregate and form a columnar structure with dipolar interactions (Fig. 7a).¹⁴² Therefore, EREs show reversible change of modulus, which is attributed to the mismatch in the dielectric constant and conductivity between the semiconducting particles.^{141,143,144} Due to the distinct properties of their constituent materials, EREs have advantages over ERFs because they have no aggregation of particles and no leakage of carrier liquid, which are two shortcomings of ERFs.^{145,146} In addition, EREs also have advantages over magnetorheological elastomers (MREs), since the latter are driven by the magnetic field, which is hard to generate without large-sized electromagnetic coils.¹⁴⁷

Filler particles play a key role in EREs by enhancing their mechanical properties. In recent years, titanium dioxide (TiO_2) or modified TiO_2 has been widely used as fillers in EREs for improved modulus.^{148,149} An ERE composed of acetylacetonate dipolar molecule-doped mesoporous aggregates of TiO_2 in a PDMS matrix has a storage modulus of 2 MPa under an electric field of 2 kV mm^{-1} , compared with 1.5 MPa without an electric field (Fig. 7b).¹⁴¹ The relative change in the elastic modulus increases with the DC electric field and decreases with the increasing AC electric field frequency. This behavior is mainly

attributed to the higher conductivity and larger relative permittivity of TiO_2 ($2.5 \times 10^{-7} \text{ S m}^{-1}$, 120) than the PDMS matrix ($1 \times 10^{-13} \text{ S m}^{-1}$, 2.7). As another example, urea-coated TiO_2 particles dispersed in silicone rubber have a storage modulus of 0.81 MPa under an electric field of 3 kV mm^{-1} , compared with 0.21 MPa without an applied electric field (Fig. 7c).¹⁵⁰ The ERE filled with urea-coated TiO_2 shows a higher storage modulus than that with bare TiO_2 (0.67 MPa), which is due to the higher dielectric constant of the former (Fig. 7d). The same group of researchers also modified the surface of TiO_2 particles with two coupling agents, 3-(trimethoxysilyl)propyl methacrylate (A174) and triethoxyvinylsilane (VTEO), to further increase the interfacial bond strength and achieved a higher dielectric constant.¹⁵¹ Due to the change of modulus in response to an electric field, EREs can be used in various applications such as control of structural vibration.^{152,153}

In summary, both electro-responsive SMP composites and IPMCs show electromechanical response, and EREs show electro-rheological response. As displayed in Table 2, a comparison between the group of SMP composites and the IPMCs shows that the latter have more rapid response under a smaller voltage. However, as mentioned in the section of photo-responsive SMP composites (Section 2.1), SMP composites can achieve more complex shape changes or motions, while IPMCs only show bending behavior under an electric field. Although applying different driving signals to different sectors of IPMCs may enable complex motions such as twisting,^{154,155} it requires sophisticated control, which can limit its practical applications in real systems. For EREs, they can be adopted to design smart devices with a

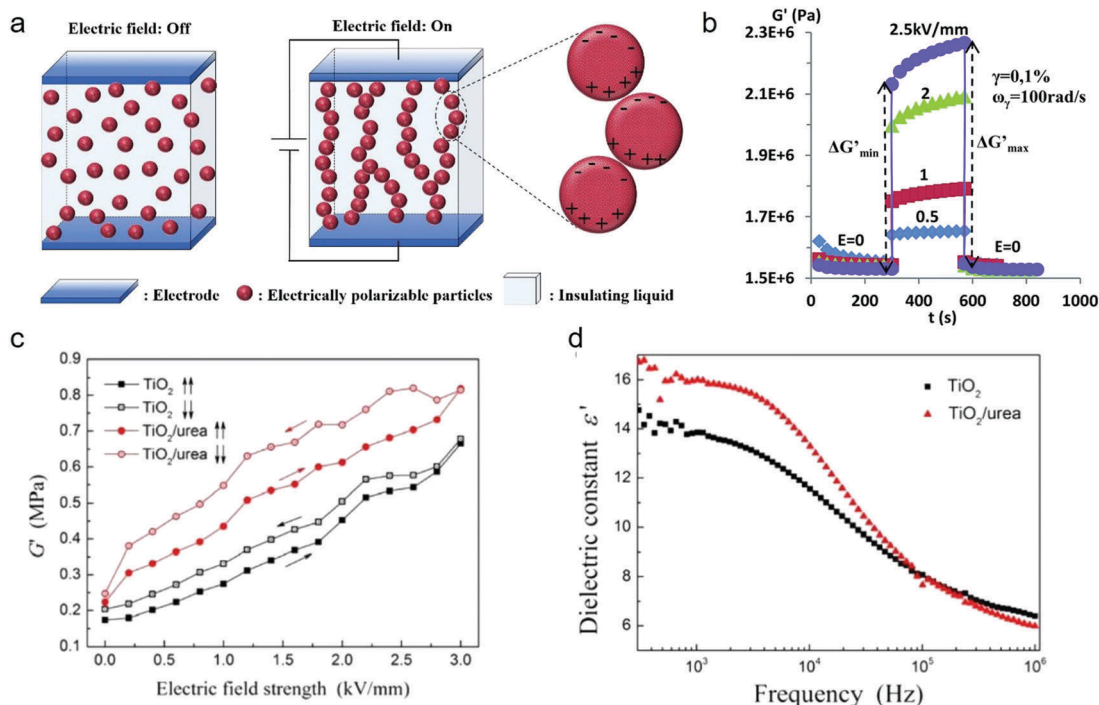


Fig. 7 (a) Schematic diagram of the ER phenomenon under an applied electric field. Reprinted with permission from ref. 142. (b) The DC electric field dependence of the storage modulus G' by applying the switching electric fields of different values. Reprinted with permission from ref. 141. Copyright 2015 Royal Society of Chemistry. (c) Storage modulus G' of elastomers filled with TiO_2 and TiO_2/urea particles as a function of electric field strength. (d) Dielectric constant as a function of the electric field frequency of elastomers filled with TiO_2 particles and TiO_2/urea particles. Reprinted with permission from ref. 150. Copyright 2015 American Chemical Society.

simple structure and low weight, such as shock absorbers,¹⁵² controlled cantilever sandwich beam,¹⁵³ and dampers.¹⁵⁶

4. Thermo-responsive polymer composites

Thermo-responsive polymer composites have been extensively explored for decades, among which the emerging positive-temperature-coefficient (PTC) composites have received great attention due to their wide applications in temperature sensors,¹⁵⁷ thermistors,¹⁵⁸ heating elements,¹⁵⁹ electrochemical storage devices,¹⁶⁰ etc. PTC composites often refer to composite materials that show an increase in electrical resistance when their temperature increases. Their operation mechanism is mainly based on the change of the percolation network of conductive filler particles in a polymer matrix upon its volume expansion or shrinkage due to temperature change. Such a temperature change can be induced by direct heating or Joule heating. The PTC intensity (the ratio of peak resistivity to room temperature resistivity) is a key parameter of PTC materials and a higher value is usually desired.¹⁶¹

The onset temperature of PTC composites is the temperature when the resistance starts to increase. Particularly, some PTC composites have a "switching temperature", beyond which their resistance increases sharply. These PTC composites are suitable for applications (e.g., thermal fuse) in which a sharp

change in resistance is required at certain temperatures. Such a rapid change can be achieved by designing the microstructure of filler particles with an optimal selection of the polymer matrix. For example, a fast and reversible thermo-responsive polyethylene (PE)/graphene-coated spiky nickel (GrNi) composite (TRPS) has been fabricated and incorporated into the electrodes of the lithium-ion battery for safe management (Fig. 8a).¹⁶² The graphene coated on the surface of Ni particles provided high electrochemical stability toward oxidation and electrolyte decomposition. Once a high temperature is induced (e.g. by a high current), the expansion of PE increases with the temperature, leading to an increased distance between Ni particles in the PE matrix and therefore causing a reduction in the electrical conductivity (Fig. 8b). This PTC material displays a high electrical conductivity of 50 S cm^{-1} at room temperature, which decreases by seven to eight orders of magnitude within 1 s upon an increase in temperature to $80\text{ }^\circ\text{C}$ (Fig. 8c). Batteries with this PTC composite built in the electrode can rapidly shut down under overheating and shorting conditions to prevent detrimental thermal runaway. After that, the batteries will cool down and are able to resume their normal functions at room temperature (Fig. 8d).

To further investigate the mechanism of the reversible and rapid response of the TRPS, impedance spectroscopy and low-temperature electrical measurements are performed to reveal the charge transport behavior of the nanopiky Ni-based nanocomposites upon temperature change.¹⁶³ The overall impedance

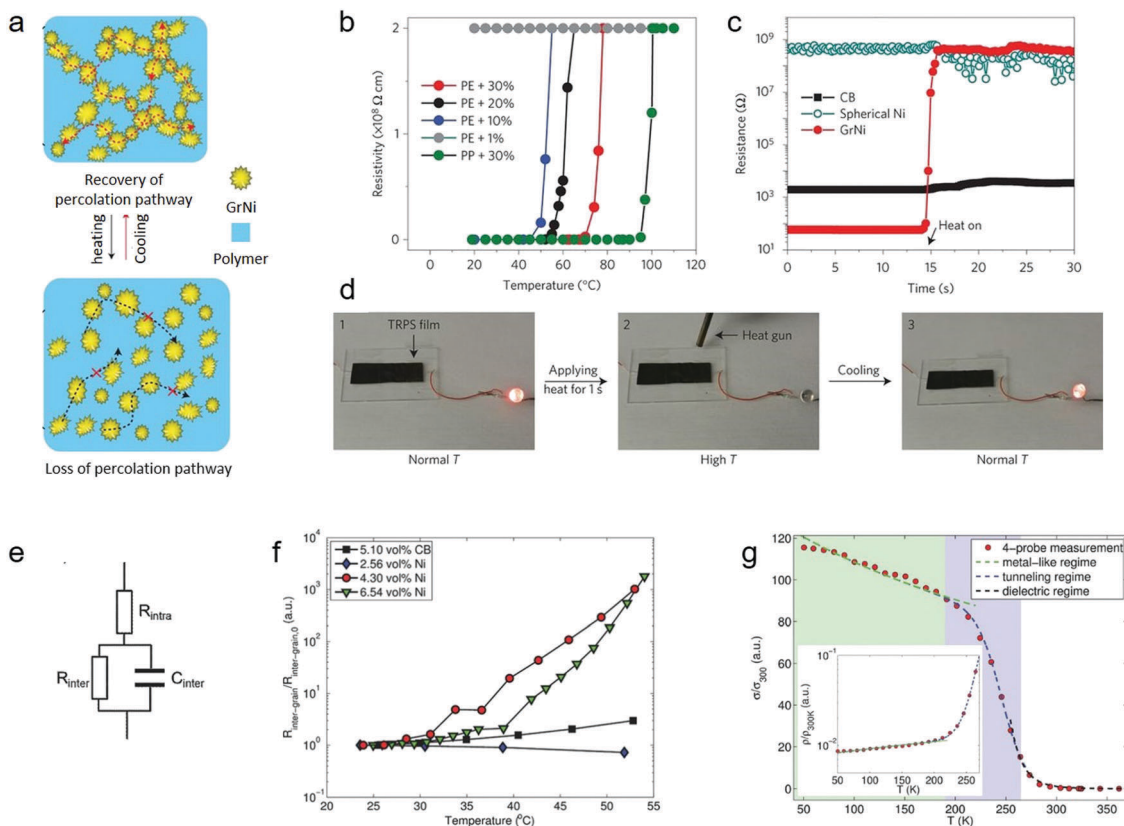


Fig. 8 (a) Thermal switching mechanism of the TRPS material. The symbol (x) illustrates blocking of electron or ion transport. (b) Resistivity changes of different TRPS films as a function of temperature, including PE/GrNi with different GrNi loadings and PP/GrNi with a 30 vol% loading of GrNi. (c) Dependence of resistance on time for PE-based composites with different conductive fillers on heating. (d) Demonstration of the thermal switching behaviour of a TRPS film using a LED connected in the circuit. Reprinted with permission from ref. 162. Copyright 2016 Springer Nature. (e) Proposed electric circuit model that describes the charge transport used to fit the measured conductivity data. (f) Temperature dependence of R_{inter} (normalized with the room temperature value at $T = 300$ K for different composites). (g) Normalized electrical conductivity–temperature dependence. $50 \text{ K} < T < 190 \text{ K}$: linearly increasing resistivity–temperature. $190 \text{ K} < T < 265 \text{ K}$: resistivity following an exponential temperature dependence. $265 \text{ K} < T < 360 \text{ K}$: stretched exponential temperature behavior. Reprinted with permission from ref. 163. Copyright 2016 John Wiley and Sons.

can be attributed to intracluster resistance (ohmic, R_{intra}), intergrain resistance (contact, R_{inter}), and capacitance (C_{inter}) in parallel with R_{inter} (Fig. 8e). As temperature increases, R_{inter} increases more significantly when the Ni volume fraction is above the percolation region, while for a similar volume fraction, the carbon black network does not show dramatic changes in R_{inter} (Fig. 8f). There are three transport regimes close to the percolation region: metal-like, tunneling, and dielectric regimes, among which the quantum tunneling effects play a major role, leading to significant interparticle resistance change upon expansion and contraction of the polymer matrix (Fig. 8g). The Ni/PE nanocomposites show adaptable electrical properties with tunable temperature sensitivity that makes them the ideal candidates for applications not only in battery safety control, but also in sensors to monitor physiological functions, where extremely small temperature variations need to be detected.¹⁵⁷

The onset temperature generally increases with increasing filler content in the PTC composites.^{162,164,165} The original gap between the adjacent fillers is smaller in PTC composites with higher filler content, and therefore requires a larger expansion for the sharp reduction of tunneling current, which means a

higher onset temperature. A mechanism study on the dependence of filler content has been performed in the ultrahigh molecular weight polyethylene (UHMWPE)/low density polyethylene (LDPE)/carbon fiber composite.¹⁶⁶ The conclusion is that filler content dependence of the onset temperature was attributed to the different size of the largest clusters.

Filler size also influences the thermo-responsive behavior of PTC composites. A high density polyethylene (HDPE)/silver coated glass flakes (AgF) composite as the model material has been studied to investigate the effect of filler size on PTC intensity.¹⁶⁷ It has been found that the PTC intensity increases with increasing filler size and decreasing filler content for both spherical and platelet-like AgFs. This is because the smaller specific surface area of larger fillers and lower filler content enable fewer possible conductive pathways, which makes it easier to disrupt the conductive network.

The polymer matrix determines the expansion/shrinkage behavior of PTC composites. The majority of the PTC composites utilize PE or PVDF as the polymer matrix because of their relatively large CTE values, such as PE/carbon black,¹⁵⁹ (HDPE)/carbon black/polyamide,¹⁶⁸ HDPE/CNT,¹⁵⁸ LDPE/carbon fiber,¹⁶⁹

poly(ethylene-co-vinyl alcohol)/carbon black,¹⁷⁰ PVDF/graphene,¹⁷¹ and PVDF/Ni¹⁶⁴ composites. Strategies such as surface modification of fillers and embedment of multiple fillers have been used to enhance the PTC properties. For example, the coupling of silane/titanate-modified carbon black and MWNTs in the HDPE matrix improves the intensity and reproducibility of the PTC effect.¹⁷² The increase in the intensity is ascribed to the anti-oxidation function of the silane or titanate coupling agents, since the oxidation of conductive particles at elevated temperature can lead to low PTC intensity. The dispersion of MWNTs can help in the reformation of the conductive paths caused by the volume expansion during the repeated heating-cooling cycles, and therefore improve the reproducibility.

In summary, PTC composites are typical representatives of thermo-responsive composites. The microstructure and volume fraction of fillers play important roles in dictating their responsive properties. Generally, the onset temperature increases with the increasing filler content, and the PTC intensity increases with the decrease of filler content and the increase of filler sizes. Although the mechanism of the PTC effect and how the properties of fillers and the polymer matrix dictate the behavior of PTC composites have been well developed, challenges lie in designing fast responsive PTC composites with superior reversibility, stability and reproducibility. In applications where an on/off switch is required, a sharp increase of the resistance upon temperature increase is desired. Due to the repeated expansion and contraction of the polymer matrix, the complete recovery of the conductive network is difficult to achieve. Therefore, rational design such as a wise selection of filler structures and surface modifications, cross-linking of polymer matrices, as well as taking advantage of the synergistic effect of multiple fillers is desired for future PTC composites to meet the requirement of various applications.

5. Conclusions and perspectives

Polymer composites that are responsive to various environmental stimuli such as light irradiation, electric field (or current) and direct heating have attracted increasing attention over the past few years. Their functional properties upon different stimuli have been extensively investigated with detailed understanding of the underlying mechanisms. Rational designs at both the material and system levels have enabled the applications of these polymer composites in many important areas. Photo-responsive polymer composites show advantages of remote manipulation and fast response. The majority of them find applications for actuators and robotics based on the photomechanical effect. For electro-responsive polymer composites, one key advantage is their easy and precise control of the applied electric field to achieve desired structure/shape changes. SMPs may be photo-responsive or electro-responsive, and the working mechanism is the photothermal and electrothermal effect, respectively. PTC composites represent the majority of thermo-responsive polymer composites. Even though the concept of PTC has existed for a few decades, the recent designs of novel filler structures

can offer unprecedented functions. Further understanding of the underlying mechanism and more creative designs of constituent materials will make PTC composites shine in emerging applications.

Despite the great advances achieved as far, there are still some major challenges in this field. Efforts are needed for a better understanding of the property-function relationship to generate sophisticated control strategies of the structure/shape change, response time and mechanical robustness. These will be the foundation for practical application of all types of polymer composites. The synthesis of new polymer matrices and filler materials as well as the design of composite architectures (multi-layer, core-shell, three-dimension, *etc.*) can lead to more intelligent and complex devices. In addition, multi-stimuli-responsive polymer composites may be fabricated by coupling different stimuli-responsive features to enhance the flexibility of control. With the future development of new materials, innovative design, and multi-stimuli coupling, one can deliver smarter systems with more functions, higher complexity and better robustness.

Conflicts of interest

The authors declare no competing financial interest.

Acknowledgements

The authors thank Prof. Shengqiang Cai for providing valuable comments and suggestions. Z. C. acknowledges the start-up fund support from The Jacob School of Engineering at University of California, San Diego.

References

- 1 Z. X. Cui, M. Zhou, P. J. Greensmith, W. K. Wang, J. A. Hoyland, I. A. Kinloch, T. Freemont and B. R. Saunders, *Soft Matter*, 2016, **12**, 4142–4153.
- 2 H. Ahmad, M. M. Rahman, M. A. Ali, H. Minami, K. Tauer, M. A. Gafur and M. M. Rahman, *J. Magn. Magn. Mater.*, 2016, **412**, 15–22.
- 3 N. Abu-Thabit, Y. Umar, E. Ratemi, A. Ahmad and F. Ahmad Abuilwaiwi, *Sensors*, 2016, **16**, 986.
- 4 G. Anton, S. Vijaya, G. Venkateshwarlu, T. Ihor, K. G. Kornev and M. Sergiy, *Adv. Funct. Mater.*, 2013, **23**, 5903–5909.
- 5 B. Monalisha, K. Amarjyoti, P. Binod, D. S. Kumar and B. Ratan, *Adv. Polym. Technol.*, 2013, **32**, E520–E530.
- 6 Z. Wang, W. Wang and D. Yu, *Chem. Eng. J.*, 2017, **330**, 146–156.
- 7 S. Yang, W. Lihuan, W. Xueqin, T. Ning, Y. Jianyong and D. Bin, *Adv. Mater.*, 2017, **29**, 1700339.
- 8 P.-C. Wang, C.-I. Chao, W.-K. Lin and S.-Y. Hung, *J. Chin. Inst. Eng.*, 2012, **35**, 595–599.
- 9 Q. Zhang, Y. Yu, K. Yang, B. Zhang, K. Zhao, G. Xiong and X. Zhang, *Carbon*, 2017, **124**, 296–307.

- 10 I. L. Liakos, A. Mondini, C. Filippeschi, V. Mattoli, F. Tramacere and B. Mazzolai, *Mater. Today Chem.*, 2017, **6**, 1–12.
- 11 M. Chen, J. Frueh, D. Wang, X. Lin, H. Xie and Q. He, *Sci. Rep.*, 2017, **7**, 769.
- 12 T. Manouras and M. Vamvakaki, *Polym. Chem.*, 2017, **8**, 74–96.
- 13 Y. W. Hao, J. X. Meng and S. T. Wang, *Chin. Chem. Lett.*, 2017, **28**, 2085–2091.
- 14 H. Shahsavan, L. Yu, A. Jakli and B. Zhao, *Soft Matter*, 2017, **13**, 8006–8022.
- 15 W. Wang, Y. Liu and J. Leng, *Coord. Chem. Rev.*, 2016, **320–321**, 38–52.
- 16 Y. J. Liu, H. Y. Du, L. W. Liu and J. S. Leng, *Smart Mater. Struct.*, 2014, **23**, 22.
- 17 T. Liu, T. Zhou, Y. Yao, F. Zhang, L. Liu, Y. Liu and J. Leng, *Composites, Part A*, 2017, **100**, 20–30.
- 18 R. Elhajjar, C.-T. Law and A. Pegoretti, *Prog. Mater. Sci.*, 2018, **97**, 204–229.
- 19 R. Weeber, M. Hermes, A. M. Schmidt and C. Holm, *J. Phys.: Condens. Matter*, 2018, **30**, 26.
- 20 H. Koerner, T. J. White, N. V. Tabiryan, T. J. Bunning and R. A. Vaia, *Mater. Today*, 2008, **11**, 34–42.
- 21 M. J. He, W. X. Xiao, H. Xie, C. J. Fan, L. Du, X. Y. Deng, K. K. Yang and Y. Z. Wang, *Mater. Chem. Front.*, 2017, **1**, 343–353.
- 22 Y. Y. Feng, M. M. Qin, H. Q. Guo, K. Yoshino and W. Feng, *ACS Appl. Mater. Interfaces*, 2013, **5**, 10882–10888.
- 23 Y. Hui, L. W. Ru, W. Ting, W. Juan, Y. Jiancan, H. Ke, Q. Dianpeng, W. Changjin and C. Xiaodong, *Adv. Mater.*, 2017, **29**, 1701627.
- 24 L. Fang, T. Y. Fang, X. X. Liu, Y. R. Ni, C. H. Lu and Z. Z. Xu, *Compos. Sci. Technol.*, 2017, **152**, 190–197.
- 25 L. Yu and H. F. Yu, *ACS Appl. Mater. Interfaces*, 2015, **7**, 3834–3839.
- 26 R. R. Kohlmeier and J. Chen, *Angew. Chem., Int. Ed.*, 2013, **52**, 9234–9237.
- 27 C. S. Li, X. Z. Huang, C. H. Li and H. R. Jiang, *Mol. Cryst. Liq. Cryst.*, 2015, **608**, 146–156.
- 28 C. S. Li, Y. Liu, X. Z. Huang, C. H. Li and H. R. Jiang, *Mol. Cryst. Liq. Cryst.*, 2015, **616**, 83–92.
- 29 L. Yu, Z. X. Cheng, Z. J. Dong, Y. H. Zhang and H. F. Yu, *J. Mater. Chem. C*, 2014, **2**, 8501–8506.
- 30 X. Y. Liu, R. B. Wei, P. T. Hoang, X. G. Wang, T. Liu and P. Keller, *Adv. Funct. Mater.*, 2015, **25**, 3022–3032.
- 31 J. D. Zhang, J. Wang, L. N. Zhao, W. L. Yang, M. Bi, Y. C. Wang, H. Y. Mu, Y. X. Li, B. S. Wang, Y. C. Gao, C. S. Li and X. Z. Huang, *Chem. Res. Chin. Univ.*, 2017, **33**, 839–846.
- 32 W. Liu, L. X. Guo, B. P. Lin, X. Q. Zhang, Y. Sun and H. Yang, *Macromolecules*, 2016, **49**, 4023–4030.
- 33 L. X. Guo, M. H. Liu, S. M. Sayed, B. P. Lin, P. Keller, X. Q. Zhang, Y. Sun and H. Yang, *Chem. Sci.*, 2016, **7**, 4400–4406.
- 34 E. Titov, L. Lysyakova, N. Lomadze, A. V. Kabashin, P. Saalfrank and S. Santer, *J. Phys. Chem. C*, 2015, **119**, 17369–17377.
- 35 W. Wang, X. M. Sun, W. Wu, H. S. Peng and Y. L. Yu, *Angew. Chem., Int. Ed.*, 2012, **51**, 4644–4647.
- 36 J. Loomis and B. Panchapakesan, *Nanotechnology*, 2012, **23**, 12.
- 37 J. Loomis, B. King and B. Panchapakesan, *Appl. Phys. Lett.*, 2012, **100**, 4.
- 38 X. M. Fan, F. Khosravi, V. Rahneshin, M. Shanmugam, M. Loeian, J. Jasinski, R. W. Cohn, E. Terentjev and B. Panchapakesan, *Nanotechnology*, 2015, **26**, 11.
- 39 F. Wang, S. H. Jia, Y. L. Wang and Z. H. Tang, *Opt. Mater.*, 2018, **76**, 117–124.
- 40 X. D. Liang, Z. C. Zhang, A. Sathisha, S. Q. Cai and P. R. Bandaru, *Composites, Part B*, 2018, **134**, 39–45.
- 41 X. Zhang, Z. B. Yu, C. Wang, D. Zarrouk, J. W. T. Seo, J. C. Cheng, A. D. Buchan, K. Takei, Y. Zhao, J. W. Ager, J. J. Zhang, M. Hettick, M. C. Hersam, A. P. Pisano, R. S. Fearing and A. Javey, *Nat. Commun.*, 2014, **5**, 8.
- 42 P. Raturi and J. P. Singh, *Sci. Rep.*, 2018, **8**, 9.
- 43 W. T. Jiang, D. Niu, H. Z. Liu, C. H. Wang, T. T. Zhao, L. Yin, Y. S. Shi, B. D. Chen, Y. C. Ding and B. H. Lu, *Adv. Funct. Mater.*, 2014, **24**, 7598–7604.
- 44 Leeladhar, P. Raturi, A. Kumar and J. P. Singh, *Smart Mater. Struct.*, 2017, **26**, 9.
- 45 R. Tang, W. Sang, Y. P. Wu, C. H. Zhu and J. Liu, *Macromol. Mater. Eng.*, 2017, **302**, 6.
- 46 Y. Hu, G. Wu, T. Lan, J. J. Zhao, Y. Liu and W. Chen, *Adv. Mater.*, 2015, **27**, 7867–7873.
- 47 Q. Ge, A. H. Sakhaei, H. Lee, C. K. Dunn, N. X. Fang and M. L. Dunn, *Sci. Rep.*, 2016, **6**, 31110.
- 48 C.-L. Huang, L. Jiao, J.-J. Zhang, J.-B. Zeng, K.-K. Yang and Y.-Z. Wang, *Polym. Chem.*, 2012, **3**, 800–808.
- 49 M. Kondo, Y. L. Yu and T. Ikeda, *Angew. Chem., Int. Ed.*, 2006, **45**, 1378–1382.
- 50 R. R. Kohlmeier, M. Lor and J. Chen, *Nano Lett.*, 2012, **12**, 2757–2762.
- 51 A. M. Smith, M. C. Mancini and S. Nie, *Nat. Nanotechnol.*, 2009, **4**, 710.
- 52 M. Meinhardt, R. Krebs, A. Anders, U. Heinrich and H. Tronnier, *J. Biomed. Opt.*, 2008, **13**, 5.
- 53 H. Zhang, H. Xia and Y. Zhao, *J. Mater. Chem.*, 2012, **22**, 845–849.
- 54 X. Kuang, K. Chen, C. K. Dunn, J. Wu, V. C. F. Li and H. J. Qi, *ACS Appl. Mater. Interfaces*, 2018, **10**, 7381–7388.
- 55 A. Lebar, G. Cordoyiannis, Z. Kutnjak and B. Zalar, in *Liquid Crystal Elastomers: Materials and Applications*, ed. W. H. de Jeu, Springer Berlin Heidelberg, Berlin, Heidelberg, 2012, pp. 147–185.
- 56 W. H. de Jeu and B. I. Ostrovskii, in *Liquid Crystal Elastomers: Materials and Applications*, ed. W. H. DeJeu, Springer-Verlag Berlin, Berlin, 2012, vol. 250, pp. 187–234.
- 57 C. Ohm, M. Brehmer and R. Zentel, in *Liquid Crystal Elastomers: Materials and Applications*, ed. W. H. DeJeu, Springer-Verlag Berlin, Berlin, 2012, vol. 250, pp. 49–93.
- 58 J. V. Selinger and B. R. Ratna, *Phys. Rev. E: Stat., Nonlinear, Soft Matter Phys.*, 2004, **70**, 041707.

- 59 Y. K. Yang, W. J. Zhan, R. G. Peng, C. G. He, X. C. Pang, D. Shi, T. Jiang and Z. Q. Lin, *Adv. Mater.*, 2015, **27**, 6376–6381.
- 60 Z. X. Cheng, T. J. Wang, X. Li, Y. H. Zhang and H. F. Yu, *ACS Appl. Mater. Interfaces*, 2015, **7**, 27494–27501.
- 61 H. Finkelmann, E. Nishikawa, G. G. Pereira and M. Warner, *Phys. Rev. Lett.*, 2001, **87**, 4.
- 62 Y. Yu, M. Nakano and T. Ikeda, *Nature*, 2003, **425**, 145.
- 63 G. S. Hartley, *Nature*, 1937, **140**, 281.
- 64 M. Wang, S. M. Sayed, L. X. Guo, B. P. Lin, X. Q. Zhang, Y. Sun and H. Yang, *Macromolecules*, 2016, **49**, 663–671.
- 65 X. Lu, H. Zhang, G. Fei, B. Yu, X. Tong, H. Xia and Y. Zhao, *Adv. Mater.*, 2018, **30**, 1706597.
- 66 S. V. Ahir and E. M. Terentjev, *Nat. Mater.*, 2005, **4**, 491.
- 67 S. Ansari, M. M. Neelanchery and D. Ushus, *J. Appl. Polym. Sci.*, 2013, **130**, 3902–3908.
- 68 S. Ansari, C. Rahima and M. N. Muralidharan, *Polym.-Plast. Technol. Eng.*, 2013, **52**, 1604–1610.
- 69 M. N. Muralidharan, K. P. Shinu and A. Seema, *Carbohydr. Polym.*, 2016, **144**, 115–121.
- 70 C. A. Tao, X. R. Zou, Z. H. Hu, H. P. Liu and J. F. Wang, *Polym. Compos.*, 2016, **37**, 1350–1358.
- 71 D. Niu, W. T. Jiang, H. Z. Liu, T. T. Zhao, B. A. Lei, Y. H. Li, L. Yin, Y. S. Shi, B. D. Chen and B. H. Lu, *Sci. Rep.*, 2016, **6**, 10.
- 72 H. Z. Liu, D. Niu, W. T. Jiang, T. T. Zhao, B. A. Lei, L. Yin, Y. S. Shi, B. D. Chen and B. H. Lu, *Sens. Actuators, A*, 2016, **239**, 45–53.
- 73 M. C. Weng, P. D. Zhou, L. Z. Chen, L. L. Zhang, W. Zhang, Z. G. Huang, C. H. Liu and S. S. Fan, *Adv. Funct. Mater.*, 2016, **26**, 7244–7253.
- 74 Y. M. Wang, H. Y. Mi, Q. F. Zheng, Z. Q. Ma and S. Q. Gong, *ACS Appl. Mater. Interfaces*, 2015, **7**, 21602–21609.
- 75 M. Y. Ji, N. Jiang, J. Chang and J. Q. Sun, *Adv. Funct. Mater.*, 2014, **24**, 5412–5419.
- 76 Y. Zhou, A. W. Hauser, N. P. Bende, M. G. Kuzyk and R. C. Hayward, *Adv. Funct. Mater.*, 2016, **26**, 5447–5452.
- 77 M. Raja, S. H. Ryu and A. M. Shanmugaraj, *Eur. Polym. J.*, 2013, **49**, 3492–3500.
- 78 T. Y. Liu, R. Huang, X. D. Qi, P. Dong and Q. Fu, *Polymer*, 2017, **114**, 28–35.
- 79 X. Wang, J. Sparkman and J. H. Gou, *Compos. Sci. Technol.*, 2017, **141**, 8–15.
- 80 M. Raja, S. H. Ryu and A. M. Shanmugaraj, *Colloids Surf., A*, 2014, **450**, 59–66.
- 81 H. B. Lu, W. L. Yin, W. M. Huang and J. S. Leng, *RSC Adv.*, 2013, **3**, 21484–21488.
- 82 H. B. Lu, J. Y. Yin, B. Xu, J. H. Gou, D. Hui and Y. Q. Fu, *Composites, Part B*, 2016, **100**, 146–151.
- 83 H. B. Lu, W. M. Huang and J. S. Leng, *Composites, Part B*, 2014, **62**, 1–4.
- 84 H. B. Lu, X. Wang, Y. T. Yao, J. H. Gou, D. Hui, B. Xu and Y. Q. Fu, *Composites, Part B*, 2015, **80**, 1–6.
- 85 H. B. Lu, S. Zhu, Y. Yang, M. H. Wei, J. Leng and S. Du, *J. Appl. Polym. Sci.*, 2015, **132**, 41673.
- 86 X. F. Liu, H. Li, Q. P. Zeng, Y. Y. Zhang, H. M. Kang, H. A. Duan, Y. P. Guo and H. Z. Liu, *J. Mater. Chem. A*, 2015, **3**, 11641–11649.
- 87 K. Wang, G. M. Zhu, F. Ren, X. G. Yan and X. P. Cui, *J. Reinf. Plast. Compos.*, 2016, **35**, 556–565.
- 88 S. S. Mahapatra, S. K. Yadav, H. J. Yoo, M. S. Ramasamy and J. W. Cho, *Sens. Actuators, B*, 2014, **193**, 384–390.
- 89 J. Alam, M. Alam, M. Raja, Z. Abduljaleel and L. Dass, *Int. J. Mol. Sci.*, 2014, **15**, 19924.
- 90 L. N. Shao, J. Dai, Z. X. Zhang, J. H. Yang, N. Zhang, T. Huang and Y. Wang, *RSC Adv.*, 2015, **5**, 101455–101465.
- 91 Q. Y. Peng, H. Q. Wei, Y. Y. Qin, Z. S. Lin, X. Zhao, F. Xu, J. S. Leng, X. D. He, A. Y. Cao and Y. B. Li, *Nanoscale*, 2016, **8**, 18042–18049.
- 92 Z. X. Zhang, W. Y. Wang, J. H. Yang, N. Zhang, T. Huang and Y. Wang, *J. Phys. Chem. C*, 2016, **120**, 22793–22802.
- 93 J. Alam, M. Alam, L. A. Dass, A. M. Shanmugaraj and M. Raja, *Polym. Compos.*, 2014, **35**, 2129–2136.
- 94 J. Alam, A. Khan, M. Alam and R. Mohan, *Materials*, 2015, **8**, 6391–6400.
- 95 H. B. Lu, F. Liang, Y. T. Yao, J. H. Gou and D. Hui, *Composites, Part B*, 2014, **59**, 191–195.
- 96 X. B. Gong, L. W. Liu, Y. J. Liu and J. S. Leng, *Smart Mater. Struct.*, 2016, **25**, 10.
- 97 S. Rana, J. W. Cho and L. P. Tan, *RSC Adv.*, 2013, **3**, 13796–13803.
- 98 M. Sabzi, M. Babaahmadi, N. Samadi, G. R. Mahdavinia, M. Keramati and N. Nikfarjam, *Polym. Int.*, 2017, **66**, 665–671.
- 99 H. B. Lu, M. Lei, C. Zhao, Y. T. Yao, J. H. Gou, D. Hui and Y. Q. Fu, *Composites, Part B*, 2015, **80**, 37–42.
- 100 H. B. Lu, M. Lei, C. Zhao, B. Xu, J. S. Leng and Y. Q. Fu, *Smart Mater. Struct.*, 2015, **24**, 8.
- 101 H. S. Luo, Z. W. Li, G. B. Yi, X. H. Zu, H. Wang, Y. J. Wang, H. L. Huang, J. W. Hu, Z. F. Liang and B. B. Zhong, *Mater. Lett.*, 2014, **134**, 172–175.
- 102 W. W. Liu, H. R. Chen, M. Q. Ge, Q. Q. Ni and Q. Gao, *Mater. Des.*, 2018, **143**, 196–203.
- 103 J. Song, J. H. Jeon, I. K. Oh and K. C. Park, *Macromol. Rapid Commun.*, 2011, **32**, 1583–1587.
- 104 Y. J. Tang, C. Chen, Y. S. Ye, Z. G. Xue, X. P. Zhou and X. L. Xie, *Polym. Chem.*, 2014, **5**, 6097–6107.
- 105 Y. Tang, Z. Xue, X. Xie and X. Zhou, *Sens. Actuators, A*, 2016, **238**, 167–176.
- 106 J. Kim, J.-H. Jeon, H.-J. Kim, H. Lim and I.-K. Oh, *ACS Nano*, 2014, **8**, 2986–2997.
- 107 J. W. Lee, Y. T. Yoo and J. Y. Lee, *ACS Appl. Mater. Interfaces*, 2014, **6**, 1266–1271.
- 108 J. Ru, Z. Zhu, Y. Wang, H. Chen and D. Li, *RSC Adv.*, 2018, **8**, 3090–3094.
- 109 A. Khan, R. K. Jain, P. Banerjee, Inamuddin and A. M. Asiri, *Mater. Res. Express*, 2017, **4**, 17.
- 110 C. Yang, Z. A. Liu, C. Chen, K. Shi, L. Zhang, X. J. Ju, W. Wang, R. Xie and L. Y. Chu, *ACS Appl. Mater. Interfaces*, 2017, **9**, 15758–15767.

- 111 O. Ozdemir, R. Karakuzu, M. Sarikanat, Y. Seki, E. Akar, L. Cetin, O. C. Yilmaz, K. Sever, I. Sen and B. O. Gurses, *Cellulose*, 2015, **22**, 3251–3260.
- 112 I. Sen, Y. Seki, M. Sarikanat, L. Cetin, B. O. Gurses, O. Ozdemir, O. C. Yilmaz, K. Sever, E. Akar and O. Mermer, *Composites, Part B*, 2015, **69**, 369–377.
- 113 M. B. El-Annaouty, M. Eid, M. Salah, E. Soliman and E. A. Hegazy, *J. Inorg. Organomet. Polym. Mater.*, 2017, **27**, 1482–1490.
- 114 S. H. Xie, Y. Y. Liu and J. Y. Li, *Appl. Phys. Lett.*, 2008, **92**, 243121.
- 115 H. B. Lu, M. Lei and J. S. Leng, *J. Appl. Polym. Sci.*, 2014, **131**, 7.
- 116 H. Lu, F. Liang, J. Gou and J. Leng, *J. Intell. Mater. Syst. Struct.*, 2015, **26**, 905–912.
- 117 B. Luo, H. Chen, Z. Zhu, B. Xie, C. Bian and Y. Wang, *Mater. Des.*, 2018, **155**, 125–133.
- 118 J. Li, W. Ma, L. Song, Z. Niu, L. Cai, Q. Zeng, X. Zhang, H. Dong, D. Zhao, W. Zhou and S. Xie, *Nano Lett.*, 2011, **11**, 4636–4641.
- 119 H. Rasouli, L. Naji and M. G. Hosseini, *Ind. Eng. Chem. Res.*, 2018, **57**, 795–806.
- 120 X. J. Xie, L. T. Qu, C. Zhou, Y. Li, J. Zhu, H. Bai, G. Q. Shi and L. M. Dai, *ACS Nano*, 2010, **4**, 6050–6054.
- 121 V. Palmre, D. Brandell, U. Maeorg, J. Torop, O. Volobujeva, A. Punning, U. Johanson, M. Kruusmaa and A. Aabloo, *Smart Mater. Struct.*, 2009, **18**, 7.
- 122 V. Palmre, E. Lust, A. Janes, M. Koel, A. L. Peikola, J. Torop, U. Johanson and A. Aabloo, *J. Mater. Chem.*, 2011, **21**, 2577–2583.
- 123 J. Kim, S.-H. Bae, M. Kotal, T. Stalbaum, K. J. Kim and I.-K. Oh, *Small*, 2017, **13**, 1701314.
- 124 R. Tiwari and E. Garcia, *Smart Mater. Struct.*, 2011, **20**, 083001.
- 125 D. N. C. Nam and K. K. Ahn, *Sens. Actuators, A*, 2012, **183**, 105–114.
- 126 Inamuddin, A. Khan, R. K. Jain and M. Naushad, *Smart Mater. Struct.*, 2015, **24**, 14.
- 127 Inamuddin, A. Khan, R. K. Jain and M. Naushad, *J. Intell. Mater. Syst. Struct.*, 2016, **27**, 1534–1546.
- 128 Inamuddin, R. K. Jain, S. Hussain and M. Naushad, *RSC Adv.*, 2015, **5**, 84526–84534.
- 129 A. Khan, Inamuddin, R. K. Jain and A. M. Asiri, *Polym. Eng. Sci.*, 2017, **57**, 258–267.
- 130 M. Annabestani, M. Maymandi-Nejad and N. Naghavi, *IEEE Trans. Electron Devices*, 2016, **63**, 1689–1695.
- 131 E. T. Enikov and G. S. Seo, *Sens. Actuators, A*, 2005, **122**, 264–272.
- 132 S. Nemat-Nasser and Y. X. Wu, *J. Appl. Phys.*, 2003, **93**, 5255–5267.
- 133 S. Nemat-Nasser, *J. Appl. Phys.*, 2002, **92**, 2899–2915.
- 134 X.-L. Wang, I.-K. Oh and T.-H. Cheng, *Polym. Int.*, 2010, **59**, 305–312.
- 135 Z. Zhu, L. Chang, K. Asaka, Y. Wang, H. Chen, H. Zhao and D. Li, *J. Appl. Phys.*, 2014, **115**, 124903.
- 136 Y. P. Seo and Y. Seo, *Langmuir*, 2012, **28**, 3077–3084.
- 137 S. Lee, C. M. Yoon, J. Y. Hong and J. Jang, *J. Mater. Chem. C*, 2014, **2**, 6010–6016.
- 138 T. Plachy, M. Sedlacik, V. Pavlinek and J. Stejskal, *J. Mater. Chem. C*, 2015, **3**, 9973–9980.
- 139 B. N. Hao, Y. X. Guo, Y. D. Liu, L. M. Wang and H. J. Choi, *J. Mater. Chem. C*, 2016, **4**, 7875–7882.
- 140 C. M. Yoon, K. Lee, J. Noh, S. Lee and J. Jang, *J. Mater. Chem. C*, 2016, **4**, 1713–1719.
- 141 A. Kossi, G. Bossis and J. Persello, *J. Mater. Chem. C*, 2015, **3**, 1546–1556.
- 142 S. Kwon, S. Piao and H. Choi, *Nanomaterials*, 2015, **5**, 2249.
- 143 T. Shiga, T. Ohta, Y. Hirose, A. Okada and T. Kurauchi, *J. Mater. Sci.*, 1993, **28**, 1293–1299.
- 144 L. Gao and X. Zhao, *J. Appl. Polym. Sci.*, 2004, **94**, 2517–2521.
- 145 X. P. Zhao and J. B. Yin, *Chem. Mater.*, 2002, **14**, 2258–2263.
- 146 Y. Dong, J. Yin and X. Zhao, *J. Mater. Chem. A*, 2014, **2**, 9812–9819.
- 147 F. Gordaninejad, X. Wang and P. Mysore, *J. Intell. Mater. Syst. Struct.*, 2012, **23**, 1033–1039.
- 148 N. Ma, Z. Q. Zhang, X. F. Dong, Q. Wang, C. G. Niu and B. G. Han, *J. Appl. Polym. Sci.*, 2017, **134**, 8.
- 149 C. G. Niu, X. F. Dong and M. Qi, *Soft Matter*, 2017, **13**, 5409–5420.
- 150 C. G. Niu, X. F. Dong and M. Qi, *ACS Appl. Mater. Interfaces*, 2015, **7**, 24855–24863.
- 151 X. F. Dong, C. G. Niu and M. Qi, *J. Mater. Chem. C*, 2016, **4**, 6806–6815.
- 152 S. S. Zhu, X. P. Qian, H. He and Q. F. Zhang, *Adv. Mater. Res.*, 2013, **641–642**, 371–376.
- 153 K. Wei, Q. Bai, G. Meng and L. Ye, *Smart Mater. Struct.*, 2011, **20**, 055012.
- 154 J.-H. Jeon, S.-W. Yeom and I.-K. Oh, *Composites, Part A*, 2008, **39**, 588–596.
- 155 K. J. Kim, D. Pugal and K. K. Leang, *Mar. Technol. Soc. J.*, 2011, **45**, 83–98.
- 156 J. M. Biggerstaff and J. B. Kosmatka, *SPIE's 9th Annual International Symposium on Smart Structures and Materials*, 2002, 4695, 6.
- 157 J. Jeon, H. B. R. Lee and Z. Bao, *Adv. Mater.*, 2013, **25**, 850–855.
- 158 Y. Zeng, G. Lu, H. Wang, J. Du, Z. Ying and C. Liu, *Sci. Rep.*, 2014, **4**, 6684.
- 159 J. H. Yoo, J. D. Han, H. J. Yoo, S. G. Ok and J. S. Ok, *Ferroelectrics*, 2017, **515**, 75–82.
- 160 H. Yang, W. R. Leow and X. Chen, *Adv. Mater.*, 2018, **30**, 1704347.
- 161 C. X. Xiong, Z. Y. Zhou, W. Xu, H. R. Hu, Y. Zhang and L. J. Dong, *Carbon*, 2005, **43**, 1788–1792.
- 162 Z. Chen, P.-C. Hsu, J. Lopez, Y. Li, J. W. F. To, N. Liu, C. Wang, S. C. Andrews, J. Liu, Y. Cui and Z. Bao, *Nat. Energy*, 2016, **1**, 15009.
- 163 Z. Chen, R. Pfattner and Z. Bao, *Adv. Electron. Mater.*, 2017, **3**, 1600397.
- 164 A. Kono, K. Shimizu, H. Nakano, Y. Goto, Y. Kobayashi, T. Ougizawa and H. Horibe, *Polymer*, 2012, **53**, 1760–1764.

- 165 H. Nakano, K. Shimizu, S. Takahashi, A. Kono, T. Ougizawa and H. Horibe, *Polymer*, 2012, **53**, 6112–6117.
- 166 R. Zhang, P. Tang, J. Li, D. Xu and Y. Bin, *Polymer*, 2014, **55**, 2103–2112.
- 167 E. Asare, J. Evans, M. Newton, T. Peijs and E. Bilotti, *Mater. Des.*, 2016, **97**, 459–463.
- 168 Y. Y. Qu, W. B. Zhang, K. Dai, G. Q. Zheng, C. T. Liu, J. B. Chen and C. Y. Shen, *Mater. Lett.*, 2014, **132**, 48–51.
- 169 W. Zhang, Y. Wan, Y. Dai, Y. Gao, C. Wang, W. Kou and X. Zhang, *Adv. Mater. Res.*, 2014, **1056**, 20–24.
- 170 E. J. Lee and E. S. Park, *Polym. Compos.*, 2017, **38**, 1462–1473.
- 171 L. H. Hong, Y. Z. Ming and G. X. Li, in *International Symposium on Materials Application and Engineering*, ed. M. Jawaid and E. R. Kenawy, EDP Sciences, Cedex A, 2016, vol. 67.
- 172 J.-W. Zha, D.-H. Wu, Y. Yang, Y.-H. Wu, R. K. Y. Li and Z.-M. Dang, *RSC Adv.*, 2017, **7**, 11338–11344.